This is a preprint, the final version is subject to change, of the American Mineralogist (MSA)
Cite as Authors (Year) Title. American Mineralogist, in press.
DOI: https://doi.org/10.2138/am-2018-6253

REVISION 2

A vibrational spectroscopic study of kernite to 25 GPa: implications for the high-pressure stability of borate polyhedra

Marcus Silva[1,*], Earl F. O'Bannon III[2], and Quentin Williams[1]

[1]Department of Earth & Planetary Sciences, University of California Santa Cruz, CA 95064 USA

[2]Physical and Life Sciences, Physics Division, Lawrence Livermore National Laboratory, Livermore, CA 94550 USA

*Present address: Department of Mineral Engineering, New Mexico Institute of Mining and Technology, Socorro, NM 87801 USA

Abstract

The Raman and infrared spectra of kernite ($Na_2B_4O_6(OH)_2 \cdot 3H_2O$) have been characterized up to ~25 and 23 GPa, respectively, to explore pressure-induced changes in a structurally novel mineral that contains mixed coordination borate groups (three-fold and four-fold), as well as both hydroxyl groups and water molecules. BO_3 and BO_4 vibrational modes are characterized in both the Raman and infrared spectra of kernite, and reassignments of some modes are made based on observed pressure shifts. Under compression to ~25 GPa, kernite undergoes three phase transitions: one initiates near ~2.5 GPa, the second occurs at ~7.0 GPa, and the third near 11.0 GPa. The first transition is characterized by a loss of both a subset of the Na-associated modes and a sharp OH peak, and is fully reversible. The second transition is characterized by the loss of most of the BO_3 modes and some of the BO_4 modes at ~7 GPa, and further broadening of the H_2O and OH peaks. This transition is partially reversible on decompression, but the Raman spectra indicate that the high-pressure structure and its reversion products are likely disordered. The third transition is characterized by the loss of most

Always consult and cite the final, published document. See http:/www.minsocam.org or GeoscienceWorld

of the Raman and infrared modes, and is not reversible on decompression. The decompression products from ~25 GPa have markedly different infrared and Raman spectra from the starting material, and appear to involve different bonding environments of boron than are present in the starting materials: thus, pressure treatment of boron-rich materials may generate novel quenchable structures. Notably, the BO_3 groups in kernite are destabilized under compression, with the BO_4 groups appearing to be more stable under compression. This shift in coordination may be endemic among borate glasses and crystalline borates under compression. The coordination conversion (and its products on decompression) is likely to be highly dependent on the detailed topology of the starting materials. Commonalities and differences between the three-fold to four-fold transitions in borate systems relative to those in carbonate systems are presented. Our results, combined with prior shock data, indicate that kernite, which may be representative of low-temperature borate minerals, can persist during impact events with peak shock pressures less than ~33 GPa, and the primary polyborate structural units involved in early ribose stabilization would thus survive most impact conditions.

Keywords: kernite, boron, high-pressure, vibrational spectroscopy

Introduction

Kernite ($Na_2B_4O_6(OH)_2{\cdot}3H_2O$) was discovered in the Mojave Desert, near the modern town of Boron, California in 1925 and was originally named rasorite (Hurlbut et al. 1973). Kernite from Boron, California is found in the lower part of an evaporite deposit as a metamorphic alteration of borax ($Na_2B_4O_5(OH)_4{\cdot}8H_2O$) in clay shales (Christ and Garrels, 1959; Barnard and Kistler, 1966; Smith, 1968; Hurlbut et al., 1973; Garrett, 1998). The Kramer borate deposit in Boron, California is the type locality of kernite. It has only been found at a few other

Always consult and cite the final, published document. See http:/www.minsocam.org or GeoscienceWorld

localities around the world, such as the Tincalayu Mine, Argentina (Hurlbut et al. 1973), Sarikaya B deposit, Turkey (García-Veigas and Helvaci 2013), and possibly in Lewis Cliff, Antarctica (Fitzpatrick et al. 2013). While not particularly common on Earth, there are strong indications of borate minerals within fluid-associated veining and evaporitic deposits on Mars, and these may be of astrobiological importance (Stephenson et al. 2013; Cloutis et al. 2016).

The crystal structure of kernite was first reported by Amoros (1945) using x-ray diffraction techniques. Due to the many light atoms comprising kernite, it has been re-investigated by many workers using single-crystal x-ray diffraction to accurately determine the H-atom positions and the coordination of the B and Na atoms (Ross and Edwards, 1959, Giese 1966, Cooper et al. 1973, Christ and Clark, 1977). Kernite crystallizes in the monoclinic $P2_1/c$ space group with four formula units in the unit cell (e.g., Cooper et al. 1973). Kernite is unusual in its crystal chemistry since it contains both trigonal planar BO_3 and tetrahedral BO_4 groups (Figure 1). The two Na sites are 6-fold coordinated by five oxygens and one water molecule (Na1) and 5-fold coordinated by two oxygens and three water molecules (Na2). The 5-fold coordinated Na sites form dimers by the sharing of two oxygens while 6-fold coordinated Na sites are linked to them by corner-sharing of one O atom. One triangular BO_2OH group and two tetrahedral BO_4 groups share corner oxygens to form six membered rings (Cooper et al. 1973). BO_4 groups link together to form chains that run parallel to the *b*-axis, which are held together by hydrogen bonding between the H_2O molecules and the OH groups.

The ambient pressure stability of kernite has been well studied (Schaller, 1930; Menzel et al., 1935; Menzel and Schulz, 1940; Pabst and Sawyer, 1948; Sennova et al. 2005). Kernite alters to tincalconite ($Na_2B_4O_7{\cdot}5H_2O$) at ambient conditions by hydration (Pabst and Sawyer,

Always consult and cite the final, published document. See http:/www.minsocam.org or GeoscienceWorld

1948). When heated in air to above ~80 ^{o}C, it partially dehydrates to $Na_2B_4O_6(OH)_2 \cdot 1.5H_2O$, at temperatures >115 ^{o}C it amorphizes, and on further heating above 525 ^{o}C, an anhydrous $Na_2B_4O_7$ phase crystallizes (Sennova et al. 2005). Spectroscopic or diffraction experiments on kernite under static compression do not appear to have been reported, and high-pressure investigations of kernite are scarce, with the exception of the shock wave study of kernite by Boslough et al. (1980) which focused on shock-induced water loss. They found that kernite did not noticeably dehydrate following impacts up to ~33 GPa, but changes in the hydrogen bonding environment were reported. Their infrared spectra of shocked and unshocked kernite indicated that changes in the bonding environment of structural and non-structural water occurred following shock, and that there was some evidence for rearrangement of the water molecules (Boslough et al. 1980). However, the behavior of the borate polyanion chains was not examined, as no spectra were reported outside of the hydroxyl stretching region. Hence, the post-shock behavior of the BO_3 and BO_4 groups as well as the Na sites is unknown.

A possible role of borates in the earliest evolution of life has been extensively discussed (Benner, 2004; Ricardo et al. 2004; Cossetti, et al., 2010; Grew et al. 2011; Saladino et al. 2011; Scorei, 2012). It has been shown experimentally that the presence of borate minerals such as colemanite ($CaB_3O_4(OH)_3 \cdot H_2O$), ulexite ($NaCaB_5O_6(OH)_6 \cdot 5H_2O$) and kernite ($Na_2B_4O_6(OH)_2 \cdot 3H_2O$) can stabilize ribose in solution against decomposition (Ricardo et al. 2004; Saladino et al. 2011), and hence act as catalysts to prebiotic syntheses (Saladino et al. 2011). The presence of borates would allow for the survival and accumulation of pre-biotic ribose from simple organic precursors (Grew et al. 2011). Interestingly, borate minerals have been shown to have little to no effect on the stability of RNA itself (Cossetti et al. 2010). However, since ribose is a

Always consult and cite the final, published document. See http:/www.minsocam.org or GeoscienceWorld

component of ribonucleic acid (RNA) and is chemically unstable, the stabilization of ribose could have been a critical step in the evolution of nucleic acids. Which borate minerals may have taken part in ribose stabilization is unclear, but colemanite, ulexite, and kernite have each been proposed (Grew et al. 2011). The oldest known ulexite and colemanite deposits are ~330 Ma while the oldest kernite deposits are ~19 Ma. Microstructures and B isotopes suggest that B-bearing evaporites were deposited in the Precambrian, and were subsequently replaced by metamorphic borates and borosilicates (Grew et al. 2011). It has been suggested that continental crust could have formed as early as 4.3 bya (Harrison, 2009; Hawkesworth et al. 2010). Thus, borate deposits could have precipitated from B-rich thermal waters in the deep past (Grew et al. 2011). Hence, the stability of kernite under high-pressure conditions is relevant for understanding the survivability of borates under high-pressures induced by meteorite impacts on both Earth and Mars (e.g., during the late heavy bombardment).

From a materials perspective, sodium borate glasses have attracted considerable interest in the materials science community due to their unusual optical and thermal properties (Krogh-Moe, 1962; Jellison and Bray, 1978; Kamitsos et al. 1987; Yano et al. 2003). These glasses are composed of polymerized structural units comprised of four distinct borate polyhedra (boroxol, petaborate, triborate, and diborate) when the alkali content is less than 33 1/3 mol% (e.g., Krogh-Moe, 1965). Interestingly, borate glasses are comprised of these well-defined and stable borate units as segments of their disordered framework (Krogh-Moe 1965; Griscom, 1978; Button et al. 1982). Indeed, some of the polyborate groupings found in borate glasses occur in related crystalline borate materials (Griscom, 1978). For example, kernite is comprised of polymerized 3-membered rings of borate polyhedra, with two tetrahedral units

Always consult and cite the final, published document. See http:/www.minsocam.org or GeoscienceWorld

forming a ring with a 3-coordinated ring (Figure 1), and the rings being linked together in chains aligned along the b-axis of this material. The pressure-induced transformations between different structural species, and particularly from the triangular BO_3 group to the tetrahedral BO_4 group have been examined under compression in glasses using NMR (Edwards et al. 2014), via molecular dynamic simulations (Kilymis et al. 2015), and following recovery from high-pressure shock-loading conditions (Manghnani et al. 2011). Additionally, a subset of the BO_3 groups in the calcium borate colemanite shift coordination at pressures above 14 GPa (Lotti et al. 2017). Hence, we are interested in whether comparable structural changes occur in crystalline kernite under compression, or whether different compressional mechanisms are accessed at higher pressure conditions by kernite. Thus, the high-pressure polymorphism of kernite may provide insights into the structural behavior of amorphous and crystalline borates under compression.

Borates such as colemanite, ulexite, and kernite have been extensively studied using vibrational spectroscopy under ambient conditions (Hibben, 1939; Krishnamurti, 1955; Weir, 1966; Vlasova and Valyashko, 1966; Maya, 1976; Maeda et al., 1979; Jun et al., 1995; Kloprogge and Frost, 1999). Early studies compared the Raman spectra of borax, kernite, and colemanite and assigned B-O vibrations (Hibben, 1939; Krishnamurti, 1955). Later studies focused on the more detailed assignment of trigonal and tetrahedral boron stretches and bends, as well as the OH and H_2O modes by comparing the spectra of these minerals. The infrared and Raman spectra of hydrated borates are complex since boron exists in both three- and four-fold coordination. These two configurations of boron have different vibrational properties; Jun et al.

Always consult and cite the final, published document. See http:/www.minsocam.org or GeoscienceWorld

(1995) and Kloprogge and Frost (1999) have relatively comprehensive assignments of the Raman and infrared spectra of kernite.

Therefore, because of its novel crystal chemistry, the importance of borates in the evolution of life, and possible relevance to the study of borate glasses, we have measured the infrared and Raman spectra of kernite to 23-25 GPa. Our experiments are oriented towards: (1) examining whether pressure induced polymorphism occurs in this phase; (2) determining if the mixed coordination Na and B sites change coordination under compression; and (3) characterizing the high-pressure behavior of hydrogen bonding within this phase and comparing it to recovered material from previous shock experiments (Boslough et al. 1980). Our net goals are to determine the stability/metastability of a complex borate mineral under high pressure and modest temperature conditions.

Experimental Methods

We used kernite from the type locality of the Kramer borate deposit, Boron, Kern County, California. The sample, UCSC collection #6141, is a large block of optical quality kernite, with dimensions of ~15 cm x 25 cm x 5 cm. Our infrared and Raman spectroscopic results are in excellent agreement with previous studies (Kloprogge and Frost 1999; Jun et al. 1995). High static pressures were generated by symmetrical and Merrill-Bassett type diamond anvil cells equipped with type Ia (Raman) and type IIa (infrared) diamonds with 500 µm, 16-sided culets. A spring steel gasket with a 200 µm hole was used as the sample compartment. Three to five ruby chips were loaded with each sample to measure the pressure using the standard ruby fluorescence method (Mao et al., 1986). All experiments were conducted at room temperature. Due to its high solubility in polar solvents, single crystals of kernite were loaded with

Always consult and cite the final, published document. See http:/www.minsocam.org or GeoscienceWorld

spectroscopic-grade KBr as the pressure medium as opposed to methanol-ethanol. We did not observe any interaction between kernite and the pressure medium over the pressure range of these experiments. Moreover, KBr has no first-order Raman spectrum, and is transparent in the mid-infrared, so no spectral contamination of the kernite spectrum is generated.

Raman spectra were collected with a Horiba LabRAM HR Evolution Raman spectrometer with a spectrometer focal length of 800 mm. Spectra were collected to a pressure of ~25 GPa at room temperature. We used an excitation wavelength of 633 nm to collect from 50-1200 cm^{-1} and an excitation wavelength of 532 nm to collect the hydroxyl stretching region from 3000-3700 cm^{-1}. An Olympus BXFM-ILHS microscope with a 50x long working distance objective was used to focus the laser beam onto the sample. We used an 1800 lines/mm grating, with a corresponding spectral resolution of ~1 cm^{-1}. We used 633 nm excitation for the low frequency modes to avoid the luminescence background generated by 532 nm excitation. No such background was observed in the higher frequency region of the spectrum, so 532 nm excitation was used in this region due to the low intensity of the OH stretches. The Raman spectrum of kernite is orientation-dependent, so variations in peak amplitudes are observed between some experiments. Spectra were collected from a laser spot size of ~2 μm and very close to the ruby used to determine pressure for each step, so we do not anticipate that pressure gradients will notably adversely affect our Raman spectra. Raman spectra were fit using a combination of Gaussian and Lorentzian functions with Horiba Labspec6 software.

We collected mid-infrared absorption spectra from room pressure to ~24 GPa at room temperature using a Bruker Vertex 70v evacuated Fourier transform infrared spectrometer (FTIR) equipped with a globar source, KBr-beamsplitter and a liquid-N_2 cooled mercury-

Always consult and cite the final, published document. See http:/www.minsocam.org or GeoscienceWorld

177 cadmium-telluride (MCT) detector. Infrared spectra were collected with a resolution of 4 cm^{-1}.
178 Kernite was ground into a powder and mixed with spectroscopic-grade KBr in a ratio of 90%
179 KBr: 10% sample by weight, with KBr serving as both an infrared window and the pressure
180 medium. Pressure gradients in our infrared experiments did not produce notable broadening of
181 our spectra relative to the ambient pressure spectrum. This is in accord with recent high-
182 pressure infrared spectra of the OH region in amphiboles that show that the full width at half
183 maximum (FWHM) of hydroxyl stretches is nearly indistinguishable between neon and KBr
184 loaded samples up to ~20 GPa (Thompson et al. 2016). Moreover, since the infrared spectra
185 were collected using an infrared beam that interacts with the entire sample compartment of
186 the DAC, we reported the average pressure determined for each pressure step using multiple
187 rubies. Under natural shock conditions, it is likely that transient differential stresses arise.
188 Hence, probing the properties of kernite with modest amounts of differential stress may have
189 relevance to structural changes induced by impact. Infrared spectra were also fit using a
190 combination of Gaussian and Lorentzian functions with Bruker OPUS software.

191 **Results**

192 *Ambient*

193 The ambient pressure Raman spectrum of kernite has over 30 resolvable peaks at room
194 pressure and temperature (Figure 2), which have been generally assigned by Kloprogge and
195 Frost (1999). Many of the lower frequency modes are related to Na-O bending and stretching
196 vibrations against the borate polyhedra. The region of the spectrum from ~390 to 1100 cm^{-1}
197 corresponds to BO_3 and BO_4 bending and stretching modes. Both symmetric and antisymmetric
198 stretches of the BO_3 and BO_4 groups have been previously assigned. There are regions of

Always consult and cite the final, published document. See http:/www.minsocam.org or GeoscienceWorld

199 overlap between modes associated with these two boron configurations, so the detailed
200 assignments of some of the observed modes are not unique. From 3200-3500 cm^{-1}, we observe
201 a broad H_2O-associated hydroxyl-stretching manifold that when deconvolved contains five
202 modes, and at ~3547 cm^{-1} a sharp stretch associated with the more weakly bound hydroxyl
203 units is observed. On the low frequency side of the broad H_2O modes, a shoulder is observed
204 near 3000 cm^{-1}, which may be an indication of strong hydrogen bonding. Two of the eight
205 crystallographically distinct hydrogens in kernite are strongly hydrogen bound, providing
206 linkages between the chains of borate rings (Cooper et al., 1973).
207 The ambient pressure mid-infrared spectrum (Figure 2) has several overlapping bands,
208 and is in good agreement with the infrared spectrum of kernite reported by Jun et al. (1995). As
209 with the higher frequency portions of the Raman spectrum, the mid-infrared spectrum is
210 composed primarily of bending and stretching modes of the BO_3 and BO_4 groups. The infrared
211 OH stretching region is similar in location and morphology to the Raman spectrum (Figure 2),
212 implying that Davydov (factor group) splitting of the O-H stretches is small at ambient pressure.
213 There is a broad H_2O-associated band that has four deconvolvable components centered near
214 3250 cm^{-1}, and an H-O-H bending mode is observed near 1701 cm^{-1}. This is substantially
215 elevated in frequency relative to that of the vibration of water in the liquid or gas phase (each
216 below 1655 cm^{-1}; Falk, 1990), which is consistent with the water molecules in kernite being
217 relatively strongly hydrogen bound to one another (Cooper et al. 1973), and hence the bending
218 vibration involving deformation of strong hydrogen bonds as well. As with the Raman spectrum,
219 there is a sharp OH stretch near 3551 cm^{-1}, and a shoulder near 3000 cm^{-1} that reflects the
220 strongest hydrogen bonding environment in kernite.

Always consult and cite the final, published document. See http:/www.minsocam.org or GeoscienceWorld

Compression

Representative Raman spectra on compression are shown in Figure 3, and the Raman mode shifts are shown in Figure 4. Under compression the Raman spectra of kernite changes dramatically. At ~2.5 GPa, three Na-associated modes initially at 113, 123, and 128 cm^{-1} disappear, as well as modes originating at 163, 175, 214, 246, 260, 308, and 346 cm^{-1} all disappear. Also at 2.5 GPa, the symmetric stretch BO_4 mode at 807 cm^{-1} disappears. Thus, a transition that appears to have major effects on the Na-polyhedra takes place near 2.5 GPa, with some associated changes in the borate groups. Table 1 lists the observed Raman modes, their assignments and pressure shifts up to the ~2.5 GPa transition. Interestingly, the lowest frequency Na-associated mode near 83 cm^{-1} shifts negatively under compression. Because of its low frequency, this could generate a soft mode transition. However, its rate of shift is not sufficiently large/non-linear enough to be the cause of the 2.5 GPa transition (Sanjurjo et al. 1983; O'Bannon et al. 2016b); it also persists through the transition. The other observed Na-associated modes shift positively under compression, and become more difficult to resolve as pressure is increased. Between 400-550 cm^{-1}, there are three distinct peaks at 428, 463 (which has two components that become resolved under compression), and 498 cm^{-1} which merge under compression at ~2.5 GPa to form a broad doublet that can be deconvolved into four peaks (at 436, 461, 481, and 510 cm^{-1} at 2.5 GPa). As Klopproge and Frost (1999) note, these modes likely correspond to BO_3 and BO_4 bending modes. The mode shifts of these peaks fall into two general categories (Table 1): those between 390 and 461 cm^{-1}, which have shifts between 1.79 and 2.58 cm^{-1}/GPa, and those at 466 and 498 cm^{-1}, which shift at faster rates of 7.43 and 4.92 cm^{-1}/GPa, respectively. Based on the differing strengths of bonding in the BO_3

Always consult and cite the final, published document. See http:/www.minsocam.org or GeoscienceWorld

and BO_4 tetrahedra, we assign the lower frequency bands to bending vibrations of the BO_4 tetrahedra, and the two higher lying features to bending of the BO_3-groups. The two bands at 557 and 581 cm^{-1} each have notably lower shifts of 1.41 and 0.69 cm^{-1}/GPa: we assign these to O-H librational modes, since such bands are known to have small pressure shifts (e.g., Scott et al. 2007), and librational modes are expected in this region for phases such as kernite with intermediate to strong hydrogen bonding (Lutz et al. 1998).

By 3.3 GPa, two of the four remaining modes in the bending region disappear, and an intense doublet with frequencies of 461 and 487 cm^{-1} remains. This doublet is relatively insensitive to compression up to ~6.5 GPa. Above ~6.5 GPa, the lower frequency peak of this doublet disappears and the higher frequency peak rapidly merges with another peak that shifts downward from 547 cm^{-1} (Figure 4a). This single band, now centered near 524 cm^{-1} at 6.5 GPa, shifts positively up to ~25 GPa. There are other notable changes at 6.5 GPa: peaks originally at 742 and 933 cm^{-1} shift discontinuously to 755 and 947 cm^{-1}, and by ~7 GPa they disappear. These two peaks are likely associated with symmetric stretches of the BO_4 and BO_3 groups, respectively, and their disappearance is probably associated with marked distortions of each group. At ~7.5 GPa, a dramatic change in the Raman spectrum occurs, and only seven well-resolved modes remain within the spectrum: all other bands broaden to the degree that they are not readily resolved, or they disappear. Near 11 GPa, modes near 600 and 720 cm^{-1} become unresolvable, and only four modes can be resolved at the maximum pressure of this study. The frequencies of these modes at ~25 GPa are 169, 195, 312, and 597 cm^{-1}. The lowest two modes are likely assigned to Na-associated vibrations, while the mode at 312 cm^{-1} could be a bending mode of substantially weakened borate polyhedra, and the mode at 597 cm^{-1} may be the

Always consult and cite the final, published document. See http:/www.minsocam.org or GeoscienceWorld

symmetric stretch of these polyhedra. The net bending and stretching frequencies lie substantially below those of BO_4 tetrahedra at ambient pressures, and these thus may represent the vibrations of a more highly coordinated boron species. In this respect, the disappearance of all bands associated with the BO_3 groups in kernite indicates that the BO_3 groups have been eliminated in the high-pressure phase. The persistence of two moderate frequency bands in the high-pressure Raman spectra implies that some regular borate polyhedra persist, but that their bonding is substantially weakened, and their coordination may be increased, relative to the low-pressure BO_4 groups. Lastly, we were unable to resolve H_2O and OH modes above ~2.5 GPa in the Raman as the peaks rapidly broadened and decreased in intensity. The OH peak at 3547.5 cm^{-1} shifts negatively under compression at -9.20 (±1.05) cm^{-1} /GPa, which suggests that there is a rapid increase in the strength of the hydrogen bonding of the most weakly hydrogen bound hydroxyls under compression.

Representative infrared spectra of kernite under compression are shown in Figure 5 and the infrared mode shifts are plotted in Figure 6. Table 2 lists the observed infrared modes, assignments, and pressure shifts up to the ~2.5 GPa transition. All of the BO_3 and BO_4 modes shift smoothly and positively under compression to the transition. At 2.5 GPa, several BO_3 antisymmetric bending modes originating at 618, 653, and 691 cm^{-1} become unresolvable. By 5.0 GPa, a symmetric BO_4 stretch originating at 760 cm^{-1} becomes unresolvable, although the antisymmetric BO_4 stretches between 960 and 1022 cm^{-1} persist throughout this pressure range. The BO_3 antisymmetric stretch that originates at 1487 cm^{-1} also becomes unresolvable by 5.0 GPa. This is the first onset of a progressive broadening and loss of all of the BO_3 antisymmetric stretching vibrations by the highest pressures of our measurements. Similar to

Always consult and cite the final, published document. See http:/www.minsocam.org or GeoscienceWorld

the Raman results, several modes in the 500-600 cm^{-1} range coalesce near 7.0 GPa, leaving only one substantially broadened mode in their place. The infrared features that persisted to the maximum pressure of this study were all substantially broadened and difficult to resolve above ~7.0 GPa, and are indicative of pervasive disordering of kernite. Near 11 GPa, the BO_3 antisymmetric stretching modes in the 1300-1500 cm^{-1} region merge into a single broad mode, which progressively decreases in amplitude and disappears by 22 GPa. Hence, the infrared spectra provide compelling evidence that the BO_3 groups are destabilized within the highest-pressure phase of kernite that we observe. At 22.2 GPa, there are roughly five discrete modes that are resolvable below 1650 cm^{-1}, with frequencies of 619, 747, 978, 1263, and 1612 cm^{-1}. The two lower frequency modes are likely produced by antisymmetric bending vibrations of borate polyhedra, and the modes at 978 and 1263 cm^{-1} are associated with antisymmetric stretches of borate polyhedra. The band at 1612 cm^{-1} is assigned to the H-O-H bend. Finally, in the OH stretching region, at ~2.5 GPa, the sharp, weakly hydrogen bound hydroxyl stretching peak broadens and drops in intensity, in a manner that is virtually identical to the Raman results (Figure 3b), and it ultimately merges into the broad H_2O hydroxyl stretching envelope. The once sharp OH mode can still be deconvolved to the highest pressures of the study, and two modes are fit to the broad hydroxyl stretching manifold to the maximum pressure of this study. The OH-stretching peak, the broad H_2O hydroxyl stretching modes, and the H-O-H mode all shift negatively under compression up to ~7.0 GPa. Above 7.0 GPa, the broad H_2O and broadened OH mode may shift slightly positively, suggesting that H-bonding may become weaker in the higher-pressure phases. The H-O-H bend shows complex behavior, shifting rapidly and positively from ~7.0 GPa to ~11.0 GPa, and above ~11.0 GPa it shifts negatively up to the

Always consult and cite the final, published document. See http:/www.minsocam.org or GeoscienceWorld

maximum pressure of this study. Since the frequency of the H-O-H bend tends to increase with decreasing H-O-H bond angle, this trend is consistent with an initial broadening of the H-O-H angle up to 7 GPa, followed by an interval of rapid contraction between 7 and 11 GPa. Above 11 GPa, it appears to resume weakly widening in the highest pressure phase.

Decompression

Representative Raman and infrared spectra on decompression are shown in Figure 7. During decompression of the Raman sample, the two peaks that persisted to ~25 GPa shift negatively and monotonically with decreasing pressure, with the primary peak moving back down to ~450 cm^{-1}. Additional bands begin to appear near ~3.2 GPa. For example, a shoulder to the high frequency side of the strongest peak appears near ~3.2 GPa on decompression and by ~0.2 GPa, it has split away from the primary peak and its peak location is at 590 cm^{-1}. Notably, a number of bands (and particularly those at low frequencies) appeared only upon full decompression of the sample (Figure 7a). Only two modes actually persist from ~25 GPa down ~10 GPa (Figure 4). Three broadened modes reappeared in the OH stretching region; however, the sharp OH stretch does not reappear.

On decompression, the infrared spectra have essentially two broad bands that can be fit with five modes, which shift negatively with decreasing pressure back to room pressure (Figure 7b). The spectrum remained broad until the sample was fully decompressed to room pressure, when a sequence of sharper modes appeared. These six sharp modes in the mid-frequency region of the infrared spectrum (~500-1500 cm^{-1}) are not as sharp as the bands in the ambient starting material that appear in this region. Notably, below 5 GPa (and particularly below 3 GPa), the BO_3-antisymmetric stretching bands between 1300-1500 cm^{-1} recover their amplitude

Always consult and cite the final, published document. See http:/www.minsocam.org or GeoscienceWorld

within the spectra: their reappearance is accompanied by shifts in amplitude in the lower frequency region between 700 and 1200 cm^{-1} (Figure 7b). In the OH region, the sharp OH peak does not return on decompression, but the broad H_2O hydroxyl-stretching bands are similar to those in the starting infrared spectrum of kernite. As with the decompressed Raman spectrum, the decompressed infrared spectrum does not resemble the initial infrared spectrum of kernite.

Fully Decompressed Product

The fully decompressed Raman sample has a spectrum that is unlike the ambient spectrum of the starting material (See supplementary Figure S1). There are two low-intensity broad peaks from 50-200 cm^{-1} and only 6 modes from 200-600 cm^{-1}, which is dramatically different from the ambient spectrum that consisted of a large number of BO_3 and BO_4 bending modes in this region. The BO_4 stretching region from 700-850 cm^{-1} is also much less complex. The prominent BO_4 symmetric stretching vibration in kernite at ~739 cm^{-1} has no analogue in the decompressed spectrum. If tetrahedral BO_4 groups are present in the decompressed material, they have a notably different local bonding environment, and may be substantially distorted. The BO_3 symmetric stretches near 950 cm^{-1} in the starting material also appear to have been profoundly affected by compression, leaving them broadened, of low intensity, and modestly elevated in frequency relative to the most prominent BO_3 symmetric stretch in the starting material. The OH stretching region from 3200-3600 cm^{-1} has completely changed its morphology. In lieu of the distinct H_2O and OH peaks in kernite, a sequence of peaks with a completely different intensity distribution and locations is observed, which can be fit with four peaks at ~3200, 3350, 3500, and 3650 cm^{-1}. In short, the fully decompressed spectrum is fundamentally different from the initial ambient spectrum in every spectral region, but the

Always consult and cite the final, published document. See http:/www.minsocam.org or GeoscienceWorld

353 presence of discrete, relatively sharp (albeit broadened) peaks suggests that the decompressed
354 product may be crystalline, and may have recrystallized on decompression to ambient
355 condition. Table 3 lists the frequencies and assignments of the Raman modes observed in the
356 spectra decompressed from ~25 GPa.

357 The infrared spectrum of the decompressed material also does not resemble the initial
358 ambient infrared spectrum. It is much less complex and most of the sharp modes have
359 broadened, and coalesced into single peaks (See supplementary Figure S2). Although the
360 maximum pressure of the infrared experiment was ~2 GPa lower than the Raman experiment,
361 we believe that they accessed similar structural states at both high pressures and on
362 decompression. The mid-infrared region from 500-1000 cm^{-1} of the decompressed product is
363 made up of only four main peaks (Table 3), whereas in the ambient spectrum there were more
364 than ten distinct peaks. The broad mode from 1300-1500 cm^{-1} associated with BO_3
365 antisymmetric stretches, has returned but sharp components in this region are not resolvable.
366 The OH stretching region of the decompressed material is, because of fringing, more difficult to
367 characterize in the infrared than in the Raman. The OH stretch near 3551 cm^{-1} has merged into
368 the H_2O stretching envelope, and a broad continuum centered near 3300 cm^{-1} is observed.

369 **Discussion**

370 ***Reversibility of observed phase transitions***

371 Our vibrational spectroscopic results clearly indicate that kernite undergoes three phase
372 transitions under compression: the first is near 2.5 GPa, a structurally more dramatic transition
373 occurs near 7.0 GPa, and the spectra become notably simpler, and possibly indicate a highly
374 disordered structure, near 11.0 GPa. Both the high-pressure Raman and infrared studies

Always consult and cite the final, published document. See http:/www.minsocam.org or GeoscienceWorld

suggest that the structure of kernite changes irreversibly under compression to ~25 GPa. To assess the reversibility of each of these high-pressure phase transitions, additional Raman experiments of pressure-quenched products were conducted (Figure 8).

A decompressed Raman spectrum of a sample of kernite compressed to ~3.1 GPa indicates that the ~2.5 GPa transition is fully reversible (Figure 8). This indicates that any compaction of the structural channels that run parallel to the *b*-axis in kernite across this transition is reversible, and changes in Na sites and hydrogen bonding geometries are fully recoverable across this transition. No changes in the coordination of the BO_3 groups occur across this transition and the H-bonding environment of the OH groups and H_2O molecules is not drastically changed. The BO_4 groups appear to be mostly unaffected by this transition.

Our Raman spectra suggest that the bonding environment of the Na sites changes dramatically above ~7.0 GPa, based on the profound changes in the spectra of the low-frequency region under compression (Figure 3). Moreover, the OH stretch broadens across this transition and particularly on its low frequency side (Figure 5), suggesting that a wider and stronger range of hydrogen-bonding environments is being introduced under compression. Ultimately, the sign of the pressure shift of the OH stretching in the infrared experiments changes from negative to positive above ~11 GPa, implying that complex hydrogen bonding geometries may be present in the high-pressure phase (such as bifurcated hydrogen bonds). Decompressed Raman spectra from 8.2 GPa indicate that the structural changes that occur across the ~7.0 GPa transition are not fully reversible, but many of the original modes do return on decompression. These modes are broadened and shifted from their ambient frequencies, suggesting that this phase transition has disordered the structure of kernite (Figure 8). And,

Always consult and cite the final, published document. See http:/www.minsocam.org or GeoscienceWorld

new bands appear in the quenched spectrum from 8.2 GPa, including the strongest feature in the spectrum near 590 cm^{-1}. These bands are not present in the starting material, and indicate that new structural environments are present in the material quenched from these conditions. Here, the decrease in amplitude of the BO_4 tetrahedral stretching peaks and the generation of a new BO_4 stretching peak near 770 cm^{-1} are consistent with a shift in coordination of one of the BO_3 groups to higher coordination in the phase that occurs above 7 GPa.

For comparison, for samples quenched from 12.4 GPa, no traces of the original kernite peaks are observed (Figure 8), and kernite has completely and irreversibly transformed to a high-pressure form. The overall morphology of this spectrum has some resemblance to the phase formed on compression above 7 GPa (Figure 3a), in the sense that it is dominated by a single peak near ~570 cm^{-1}. This peak is likely associated with a bending vibration of BO_4 polyhedra, lying at higher frequency than the corresponding bonding environment in the initial kernite. If the peaks near 750 cm^{-1} in the material quenched from 12 GPa represent symmetric stretches of BO_4 units, then the bending force constants of the BO_4 tetrahedra are substantially elevated in the quenched material, while those of the stretching vibrations are not greatly altered. This implies that the geometry of the polymerized tetrahedra in the quenched material (and possibly in the 7-11 GPa phase, as well) is such that the tetrahedral symmetric bending vibration may involve a substantial stretching component of adjoining O-B bonds.

Finally, for the sample quenched from 25.3 GPa, the spectrum is entirely different, implying that the structural changes that proceed above 11 GPa progressively disorder kernite. On decompression, its structure reverts to a material that is markedly different from that of the starting material. Indeed, the decompressed material from the highest pressure conditions

Always consult and cite the final, published document. See http:/www.minsocam.org or GeoscienceWorld

(Figure 8) also differs markedly in its spectrum from those of the phases generated at any conditions on compression (Figure 3a). The broad bands between 580-730 cm^{-1} may reflect a combination of the BO_4 bending and stretching vibrations of a high density, polymerized configuration. We have no simple explanation for the sharpness of the lower frequency features between 200 and 500 cm^{-1} in this highest pressure quenched material, beyond noting that this quenched phase may have more ordered domains within it (or might even be crystalline) and/or the environments of the BO_4 tetrahedra around the Na ions are such that vibrations associated with rotations of tetrahedra/Na-site deformations occur in ordered local environments.

Structural response of kernite to pressure

Initially, the structure of kernite (Figure 1) likely accommodates compression dominantly by compaction of the structural channels that run parallel to the *b*-axis, as well as compression of the Na-sites. At higher pressures (>2.5 GPa), changes in the BO_3 and BO_4 tetraborate groups likely play a major role in the compression mechanism of kernite. And, the initially weakly bound H2 hydrogen that is oriented along the a-axis (Cooper et al., 1973), and which likely generates the strong O-H stretching peak, becomes much more strongly hydrogen bound. As pressure is increased above ~7.0 GPa, the structural channels are likely substantially compacted, and the BO_3 groups likely change coordination to BO_4 groups as the structural chains become more polymerized. It is also possible that bonding between the tetraborate chains may occur above this pressure, which could result in a stiffer three-dimensional structure. As the pressure is increased above ~11.0 GPa, cross-channel bonding may initiate which could lead to disordering of the chains, and extensive disordering of the Na sites likely

Always consult and cite the final, published document. See http:/www.minsocam.org or GeoscienceWorld

441 occurs. Finally, the BO_3 groups almost entirely change coordination to BO_4 groups, and the BO_4
442 groups themselves may become more distorted. The coordination of the BO_4 groups may
443 become poorly defined at the highest pressures of these experiments; this lack of definition, as
444 manifested by the markedly enhanced breadth of the likely B-O stretching vibrations (Figure 5)
445 also coincides with a weakening of H-bonding above ~11 GPa. This weakening of O-H bonding
446 associated with water molecules at high pressures is compatible with either the onset of
447 positive, or possibly decreasing negative mode shifts of bound water at high pressures in other
448 3-fold cation bearing phases such as trona and ikaite (O'Bannon et al. 2014; Shahar et al. 2005).
449 This decrease, or decrease in the rate of increase, of hydrogen bonding with pressure may be
450 associated with the comparatively rigidly shaped water molecule not being able to topologically
451 access strong, linear hydrogen bonds within complex, geometrically shifting, compacting
452 surroundings.

453 Notably, the mid infrared spectra probe only vibrations of the BO_3, BO_4, H_2O and OH
454 groups. Thus, the infrared spectra provide little information on the bonding environment of the
455 Na sites under compression. Only the low-frequency Raman spectra provide primary
456 constraints on the Na bonding. Our infrared and Raman results are both consistent and
457 complementary with one another. Within the infrared spectra, the BO_3 modes and the OH
458 stretch persist to higher pressures than they do in the Raman experiments, which is a reflection
459 of the differences in sensitivity between the two techniques—for example, it is likely that the
460 infrared experiments are more sensitive to lower symmetry, distorted BO_3 groups.

461 *Decompressed products*

Always consult and cite the final, published document. See http:/www.minsocam.org or GeoscienceWorld

462 The sharp features observed in the decompressed Raman and infrared spectra suggest
463 that the decompressed products are substantially more ordered than kernite at high pressures,
464 and the quenched products may be crystalline (Figures 9 and 10). The decompressed structure
465 likely contains some BO_3 groups (Table 3), although the weakness of the BO_3 stretching peaks in
466 the Raman spectra indicate that these may be quite distorted. The channels that contain the
467 H_2O molecules have likely undergone extensive rearrangement. Most of the boron in the
468 decompressed structure is probably tetrahedrally coordinated, but these tetrahedra, along with
469 the OH groups, may also be distorted. Kernite has chains of BO_4 tetrahedra and sodium sites
470 running parallel to the *b*-axis with trigonal BO_3 sites branching off of them (Figure 1). This
471 creates channels in the structure that are held together by hydrogen bonding. The collapse of
472 these channels likely allows oxygen atoms from the adjacent channel to move into the
473 coordination sphere of an adjacent BO_3 group. Moreover, the transition of the BO_3 groups to
474 BO_4 groups likely substantially changes the geometry of the Na sites, which are relatively
475 distorted in the kernite starting material. Interestingly, the lowest frequency region in the
476 Raman spectrum of the decompressed material is notably featureless and only two very low
477 intensity broad modes are observed near 124 and 168 cm^{-1}. We speculate that the two Na sites
478 might have converged on the same coordination (at ambient conditions the Na sites are 5- and
479 6-fold coordinated).

480 We note one novel aspect of the pressure-induced mode shifts that we observe in
481 kernite. A general scaling of mode Gruneisen parameter with mode frequency has long been
482 recognized in molecular crystals (e.g., Zallen 1974) and in silicates (Williams et al. 1987). The
483 basic concept is that weaker bonds give rise to lower frequency vibrations and larger mode

Always consult and cite the final, published document. See http:/www.minsocam.org or GeoscienceWorld

Gruneisen parameters. Figure 9 shows such a scaling for the mode shifts of kernite: clearly, above ~150 cm^{-1}, this general trend of decreasing mode Gruneisen parameter with increasing frequency is obeyed. Below 150 cm^{-1}, this overarching trend is clearly violated in kernite. Our simple explanation for this unexpected trend is that the structural complexity of kernite gives rise to low-frequency modes that, while not all soft, are not as fully "hard" as would be expected from simple systematics. The ramifications of this are that kernite has a range of low-frequency vibrational motions that are oriented such that, under compression, they reflect a normal coordinate along which the geometry of the kernite lattice might be susceptible to irreversible deformations. And, this simple explanation implicitly involves a broad suite of possible phase transitions that are not fully favored that the kernite lattice could undergo. This in turn is in loose accord with our observation of extensive polymorphism on both compression and decompression of the kernite lattice.

Implications

a. Why does the coordination change from BO_3 to BO_4 occur readily, while the CO_3 to CO_4 transition does not?

The energetic difference between the BO_3 and BO_4 configurations is known to be relatively small within boron-bearing oxide glasses: changes in fictive temperature/cooling rate or modest changes in pressure (less than 2 GPa) can modulate the relative amounts of these two structural species (e.g., Gupta and Tossell, 1981; Wondraczek et al. 2007; Edwards et al. 2014; Smedskjaer et al. 2014). Within crystalline borates, the fixed topology of the starting material might be expected to modulate the pressure range over which BO_3 groups are destabilized under static pressures relative to BO_4 groups. In kernite, it appears that the BO_3

Always consult and cite the final, published document. See http:/www.minsocam.org or GeoscienceWorld

groups are progressively eliminated at pressures above ~7 GPa, with their last spectroscopic vestige becoming unresolvable at ~22 GPa. For comparison, the calcium borate, colemanite, has half of its BO_3 groups convert to four-fold coordination at 14 GPa (Lotti et al. 2017). Thus, the destabilization of BO_3 groups appears to occur at pressures above 7 GPa in borate crystals, extending to near 22 GPa. Interestingly, this pressure range is in accord with the conversion interval of BO_3 to BO_4 groups in B_2O_3 glass under compression (Lee et al. 2005). This similarity in pressure ranges may reflect that the polyborate units which comprise the crystals are also primary components of the glasses as well, and it is the instability of the polyborate units at 300 K that may govern the pressure range over which interconversion takes place.

For comparison, compression of carbonates reveals that the CO_3 groups transform to CO_4 under very high-pressure conditions(80 to 115 GPa), and often only at high temperatures (Boulard et al. 2015; Merlini et al. 2017; Lobanov et al. 2017; Vennari and Williams 2018). This is in contrast to what is observed in borate minerals where the BO_3 groups destabilize at relatively low pressures (e.g. ~7 GPa) and transform to BO_4 groups at ambient temperatures (Lotti et al. 2017, and this study). Beyond the empirically-documented small energetic difference, why do BO_3 groups convert to BO_4 groups readily while the 3-fold carbonate group only converts to four-fold coordination at extreme pressures, with large kinetic hindrances? It is notable that the respective B-O bond distances in BO_4 and BO_3 groups are roughly 1.46 and 1.36 Å, respectively (e.g., Shannon,1976), or 7% different. Although the mechanism of the CO_3 to CO_4 transition may differ markedly between different carbonates (e.g., Lobanov et al. 2017; Vennari and Williams 2018), the transition between a 3- and 4-fold carbon-bearing phase at 105 GPa in the $CaCO_3$ system is associated with respective C-O bond distances of 1.228 and 1.315 Å (Lobanov

Always consult and cite the final, published document. See http:/www.minsocam.org or GeoscienceWorld

et al. 2017), or a change of 7% in bond distance across the coordination change. Interestingly, the estimated C-O bond distance for CO_4 groups at ambient pressure is near 1.50 Å, and that of CO_3 groups is ~1.28 Å (Shannon 1976), for a 17% difference in bond distance. Accordingly, it appears that a higher compressibility of CO_4 groups (in the metastable, low-pressure regime) relative to CO_3 groups ultimately brings the bond length difference down to 7% near 105 GPa, thus converging on a value where the conversion between XO_3 and XO_4 groups happens in both the boron and carbon systems.

The interconversion between 3- and 4-fold coordination near a 7% bond length difference in these two systems can be rationalized as being associated with geometric effects that are intimately tied to Pauling's first rule (Pauling 1960). Assuming an oxygen radius that is independent of coordination, and Pauling's minimum radius ratios for both triangular and tetrahedral coordination (0.155 and 0.225, respectively), then the ratio of the bond distances in the two different coordinations at the minimum radius ratios for the two geometries is 1.06: notably close to the 7% difference in bond distances when 3- to 4-fold interconversion is empirically observed to readily occur. The net conclusion here from this analysis is that 3- to 4-fold conversion may occur when the radius of the cations in two different coordinations is such that they obey the 'no-rattle' rule in both coordinations.

This simplistic bond-length analysis does not, of course, incorporate the detailed topologies of different crystalline phases, the critical role of second-neighbor interactions, nor the markedly different kinetic hindrances in different systems (boron shifts coordination readily at 300 K; carbon appears to require high temperatures to fully shift coordination). The ambient structure variability that is observed in borates is most similar to silicates (e.g. phylloborates,

Always consult and cite the final, published document. See http:/www.minsocam.org or GeoscienceWorld

inoborates, tektoborates). The energy curve of an Si_2O_7 group as a function of Si-O-Si angle is relatively flat over a broad angular range from ca. 120-180° (Gibbs et al. 2001; Oganov et al. 2008). A survey of borate mineral structures reveals that the inter-tetrahedral angle B-O-B angle shows a flexibility that may be slightly less than silicates, with values as low as 108.78^o and as high as 133.83^o (See supplementary Table S1 for the table of borates surveyed, and Figure S3). This suggests that the energy curve of B_2O_7 groups as a function of B-O-B angle is also relatively flat over a broad angular range, with a somewhat smaller flat range than silicates. Notably, energy calculations for borate tetrahedral B-O-B angles are sparse (Takada et al. 1995). This relatively broad angular range contrasts with what has been reported for the energy of C_2O_7 groups as a function of C-O-C angles, which show two complementary, quite narrow energetic minima (~ 5-10° wide) at 124 and 236° (Oganov et al. 2008). Hence, borate groups likely behave more similarly to silicate groups under high-pressure and temperature conditions, and it appears that the angular variability associated with different T-O-T linkages likely decreases in the order Si-O-Si > B-O-B > C-O-C. This narrow angular variability of the C-O-C linkage may prevent the structural flexibility that is observed in silicates and borates, and require reconstructive transformations on conversion to tetrahedrally coordinated phases. Hence, the kinetic barriers to tetrahedral carbon formation may be associated with the topological constraints produced by the narrow bond angles required by the energetics of the C-O-C linkage.

b. Stability of Borates Under Shock-Loading and on the Early Earth

From a broader Earth sciences perspective, while kernite is not an abundant mineral on the surface of the Earth today, it belongs to a family of minerals that may have played an

Always consult and cite the final, published document. See http:/www.minsocam.org or GeoscienceWorld

572 important role in the development of life on Earth. Kernite, colemanite and ulexite are
573 comprised of several polyborate structures such as triborate ($B_3O_3(OH)_4^-$ or $B_3O_3(OH)_5^{2-}$),
574 pentaborate ($B_5O_6(OH)_4^-$), and tetraborate ($B_4O_5(OH)_4^{2-}$). Borate is found as both BO_3 and BO_4
575 groups in the crystal structures of each of these complex minerals: as such, the behavior of
576 kernite may be generally representative of the behavior of mixed coordination low-
577 temperature boron-bearing phases. Borates such as colemanite, ulexite, and kernite have been
578 reported to stabilize ribose (e.g. Grew et al. 2011; Ricardo et al. 2004; Saladino et al. 2011).
579 Colemanite, ulexite, and kernite contain relatively high, and comparable, concentrations of
580 boron: 15.8, 13.3, and 14.9 wt.%, respectively. Hence, the polyborate structures that stabilize
581 ribose are abundant in these complex borate minerals. The mechanisms through which these
582 minerals stabilize the pentose sugar (and nucleic acid precursor) ribose are complex, but it
583 involves the dissolution of these minerals into solution, and formation of pentose-polyborate
584 complexes that are stable in solution relative to the free sugars (e.g., Ricardo et al., 2004). The
585 key contribution of these minerals is that they provide a means for concentrating boron (an
586 element present at ~0.001% abundance in Earth's crust) sufficiently that borate-induced ribose
587 stabilization can occur. When these minerals dissolve, a distribution of borate species in
588 solution is established (e.g. orthoborate, triborate, pentaborate, or tetraborates). Factors such
589 as the composition of the starting material, temperature, water-rock ratio and acidity will, of
590 course, determine what species are present and their concentrations. Since kernite is used
591 extensively in industrial applications to produce other refined borates, its solution chemistry is
592 fairly well characterized under a range of conditions (e.g., Schubert 2003, and references
593 therein). Indeed, the abundance of polyborate species strongly depends on the concentration

Always consult and cite the final, published document. See http:/www.minsocam.org or GeoscienceWorld

of boron in solution (e.g., Schubert, 1983; Felmy and Weare 1986), with higher boron concentrations favoring polyborate species. Thus, the key aspect of borate minerals is that their presence allows abundant polyborate anions, with their influence on the stabilization of ribose and other sugars, to be stable within fluids coexisting with these minerals. Thus, the ability of borate minerals to persist under high-pressure conditions implies that these minerals are likely stable under a broad range of environments (assuming that temperatures are not excessive) such as those on the heavily-impacted early Earth.

The effect of high-pressure on the stability of borate polyanions in kernite has implications for the survivability of complex borate minerals during meteorite impacts. Our Raman and infrared results suggest that kernite undergoes irreversible structural changes under compression to ~25 GPa. The decompressed Raman and infrared spectra suggest that the recovered product is ordered, and that most of the BO_3 groups have transformed to BO_4 groups, and that the OH groups are disordered. The solubility of these high-pressure phases of kernite (or their pressure-quenched equivalents) are not known. However, we expect that the solubility of these pressure-quenched phases, would be enhanced relative to non-pressure treated phases. Moreover, the solubility of pressure-disordered borates would likely be greater than that of crystalline kernite. Hence, this enhanced solubility of shock-disordered borates could enhance the rate of ribose stabilization, and hence ribose accumulation in the early Earth.

Before ~4 Gyr, it is likely that no substantial region of the Earth's surface would have survived that had been untouched by impacts (Marchi et al. 2014). If kernite, colemanite, or ulexite were present as evaporites on the early Earth, they would, inevitably, have experienced high-pressure conditions from meteorite impacts. Our results suggest that most of the BO_3

Always consult and cite the final, published document. See http:/www.minsocam.org or GeoscienceWorld

616 groups in kernite would transform to BO_4 groups and the Na-sites would become substantially
617 disordered during pervasive impacts of the late heavy bombardment. Importantly, kernite
618 would not have been completely destroyed during impact events that did not produce marked
619 heating (which the shock measurements of Boslough et al. (1980) imply includes impact events
620 with peak pressures less than 30 GPa). Hence, the primary polyborate structural units that are
621 involved with ribose stabilization would survive all but the largest impact events. Therefore, we
622 suggest that highly soluble, BO_4-dominated disordered borates would, due to both their
623 enhanced solubility and the high borate content (and thus polyborate ion concentration) of
624 their coexisting solutions, enhance the stabilization of nucleic acid precursors like ribose, thus
625 aiding in life's rocky start.

626 **Acknowledgments**

627 We thank R.L. Frost, two anonymous reviewers and the AE (M. Mookherjee) for helpful
628 comments that improved the quality of the manuscript. We also thank Dan Sampson for
629 invaluable technical assistance with the Raman and infrared spectrometers. Work partially
630 supported by NSF through EAR-1215745 and -1620423, and COMPRES, the Consortium for
631 Materials Properties Research in Earth Sciences under NSF Cooperative Agreement EAR 11-
632 57758. A portion of this work was performed under the auspices of the U.S. Department of
633 Energy by Lawrence Livermore National Laboratory under Contract DE-AC52-07NA27344.

634

Always consult and cite the final, published document. See http:/www.minsocam.org or GeoscienceWorld

References

Amoros, J.L.P. (1945) La estructura de la kernita. *Euclides, 57-58,* 599-608.

Barnard, R.M., and Kistler, R.B. (1966) Stratigraphic and structural evolution of the Kramer sodium borate ore body, Boron, California. In *Second Symposium on Salt* (Vol. 1, pp. 133-150).

Benner, S.A. (2004) Understanding nucleic acids using synthetic chemistry. *Accounts of Chemical Research*, *37*, 784-797.

Boslough, M.B., Weldon, R.J. and Ahrens, T.J. (1980) Impact-induced water loss from serpentine, nontronite, and kernite. *Proceedings of the Lunar and Planetary Science Conference, 11,* 2145-2158.

Boulard, E., Pan, D., Galli, G., Liu, Z., and Mao, W.L. (2015) Tetrahedrally coordinated carbonates in Earth's lower mantle. *Nature Communications, 6,* 6311.

Button, D.P., Tandon, R., King, C., Velez, M.H., Tuller, H.L., and Uhlmann, D.R. (1982). Insights into the structure of alkali borate glasses. *Journal of Non-Crystalline Solids*, *49*, 129-142.

Christ, C.L., and Clark, J.R. (1977) A crystal-chemical classification of borate structures with emphasis on hydrated borates. *Physics and Chemistry of Minerals*, *2*, 59-87.

Christ, C.L., and Garrels, R.M. (1959) Relations among sodium borate hydrates at the Kramer deposit, Boron, California. *American Journal of Science*, *257*, 516-528.

Cloutis, E., Berg, B., Mann, P., and Applin, D. (2016) Reflectance spectroscopy of low atomic weight and Na-rich minerals: Borates, hydroxides, nitrates, nitrites and peroxides. *Icarus, 264,* 20-36.

Cooper, W.F., Larsen, F.K., Coppens, P., and Giese, R.F. (1973) Electron population analysis of accurate diffraction data. V. Structure and one-center charge refinement of the light-atom mineral kernite, $Na_2B_4O_6(OH)_2{\cdot}3H_2O$. *American Mineralogist, 58,* 21-31.

Cossetti, C., Crestini, C., Saladino, R., and Mauro, E.D. (2010). Borate minerals and RNA stability. *Polymers*, *2*, 211-228.

Edwards, T., Endo, T., Walton, J.H., and Sen, S. (2014) Observation of the transition state for pressure-induced BO_3 -> BO_4 conversion in glass. *Science, 345,* 1027-1029.

Falk, M. (1990) Frequencies of H-O-H, H-O-D, and D-O-D fundamentals in liquid water. *Journal of Raman Spectroscopy, 21,* 563-567.

Felmy, A.R. and Weare, J.H. (1986) The prediction of borate mineral equilibria in natural waters: Application to Searles Lake, California. *Geochimica et Cosmochimica Acta, 50*, 2771-2783.

Always consult and cite the final, published document. See http:/www.minsocam.org or GeoscienceWorld

669 Filatov, S. K., & Bubnova, R. S. (2008) Structural mineralogy of borates as perspective materials
670 for technological applications. In *Minerals as Advanced Materials I* (pp. 111-115).
671 Springer, Berlin, Heidelberg.
672
673 Fitzpatrick, J.J., Muhs, D.R., and Jull, A.J.T. (1990) Saline minerals in the Lewis Cliff ice tongue,
674 Buckley Island quadrangle, Antarctica. *Contributions to Antarctic Research I*, 57-69.

675 García-Veigas, J., and Helvacı, C. (2013) Mineralogy and sedimentology of the Miocene
676 Göcenoluk borate deposit, Kırka district, western Anatolia, Turkey. *Sedimentary*
677 *Geology*, *290*, 85-96.

678 Garrett, D.E. (1998) *Borates: handbook of deposits, processing, properties, and use*. Academic
679 Press, New York.

680 Gibbs, G.V., Boisen, M.B., Beverly, L.L. and Ross, K.M. (2001) A computational quantum
681 chemical study of the bonded interactions in earth materials and structurally and
682 chemically related molecules. *Reviews in Mineralogy and Geochemistry, 42,* 345-381.

683 Giese, R.F. (1966). Crystal structure of kernite, $Na_2B_4O_6(OH)_2 \cdot 3H_2O$. *Science*, *154*, 1453-1454.

684 Grew, E.S., Bada, J.L., and Hazen, R.M. (2011) Borate minerals and origin of the RNA
685 world. *Origins of Life and Evolution of Biospheres*, *41*(4), 307-316.

686 Grew, E. S., Dymek, R. F., Hoog, J. C. M. De, Harley, S. L., Boak, J., Hazen, R. M., & Yates, M. G.
687 (2015). Boron isotopes in tourmaline from the ca. 3.7–3.8 Ga Isua supracrustal belt,
688 Greenland: Sources for boron in Eoarchean continental crust and seawater, *Geochimica*
689 *et Cosmochimica Acta*, *163*, 156–177.

690 Griscom, G.L., (1978) in: Borate glases: structure, properties, applications, eds., L.D. Pye, V.D.
691 Frechette and N.K. Kreidl, Plenum, New York.
692
693 Gupta, A., & Tossell, J. A. (1981). A theoretical study of bond distances, X-ray spectra and
694 electron density distributions in borate polyhedra. *Physics and Chemistry of Minerals*, *7*,
695 159-164.

696 Harrison, T.M. (2009). The Hadean crust: evidence from> 4 Ga zircons. *Annual Review of Earth*
697 *and Planetary Sciences*, *37*, 479-505.

698 Hawkesworth, C. J., Dhuime, B., Pietranik, A.B., Cawood, P.A., Kemp, A.I.S., and Storey, C.D.
699 (2010) The generation and evolution of the continental crust. *Journal of the Geological*
700 *Society*, *167*, 229-248.

701 Hibben, J. (1939) The Raman effect and its chemical applications. With a theoretical discussion
702 by James H. Hibben and Edward Teller. American Chemical Society, Monograph Series,
703 No. 80. Reinhold, New York.

Always consult and cite the final, published document. See http:/www.minsocam.org or GeoscienceWorld

Hurlbut, C.S., Aristara. L.F, and Erd, R.C. (1973) Kernite from Tincalayu, Salta, Argentina. *American Mineralogist*, *58*, 308-313.

Jellison, G.E., and Bray, P.J. (1978). A structural interpretation of ^{10}B and ^{11}B NMR spectra in sodium borate glasses. *Journal of Non-Crystalline Solids*, *29*, 187-206.

Jun, L., Shuping, X., and Shiyang, G. (1995) FT-IR and Raman spectroscopic study of hydrated borates. *Spectrochimica Acta Part A: Molecular and Biomolecular Spectroscopy*, *51*, 519-532.

Kamitsos, E.I., Karakassides, M.A., and Chryssikos, G.D. (1987) Vibrational spectra of magnesium-sodium-borate glasses. 2. Raman and mid-infrared investigation of the network structure. *Journal of Physical Chemistry*, *91*, 1073-1079.

Kilymis, D.A., Delaye, J.-M., and Ispas, S. (2015) Behavior of sodium borosilicate glasses under compression using molecular dynamics. *Journal of Chemical Physics, 143,* 094503.

Kim, H. J., and Benner, S. A. (2010). Comment on "The silicate-mediated formose reaction: Bottom-up synthesis of sugar silicates". *Science*, *329*, 902-902.

Kloprogge, J.T., and Frost, R.L. (1999) Raman microscopic study of some borate minerals: Ulexite, kernite, and inderite. *Applied spectroscopy*, *53*, 356-364.

Krogh-Moe, J. (1962) Structural interpretation of melting point depression in the sodium borate system. *Physics and Chemistry of Glasses*, *3*, 101-110.

Krogh-Moe, J. (1965). Interpretation of infra-red spectra of boron oxide and alkali borate glasses. *Physics and Chemistry of Glasses*, *6*, 46.

Krishnamurti, D. (1955) Raman spectra of borax, kernite and colemanite. *Proceedings of the Indian Academy of Sciences A. 41*, 7-11.

Lee, S.K., et al. (2005) Probing of bonding changes in B_2O_3 glasses at high pressure with inelastic x-ray scattering. *Nature Materials, 4,* 851-854.

Lobanov, S., et al. (2017) Raman spectroscopy and X-ray diffraction of sp^3 $CaCO_3$ at lower mantle pressures. Physical Review B, 96, 104101.

Lotti, P., et al. (2017) High-pressure induced phase transition of $CaB_3O_4(OH)_3$ H_2O (colemanite). *Journal of the American Ceramic Society, 100,* 2209-2220.

Lutz, H., Jung, C., Mortel, R., Jacobs, H. and Stahl, R. (1998) Hydrogen bonding in solid hydroxides with strongly polarizing metal ions, β-$Be(OH)_2$ and ε-$Zn(OH)_2$. *Spectrochimica Acta, 54,* 893-901.

Always consult and cite the final, published document. See http:/www.minsocam.org or GeoscienceWorld

Marchi, S., Bottke, W.F., Elkins-Tanton, L.T., Bierhaus, M., Wuennemann, K., Morbidelli, A., and Kring, D.A. (2014) Widespread mixing and burial of Earth/'s Hadean crust by asteroid impacts. *Nature*, *511*, 578-582.

Maeda, M., Hirao, T., Kotaka, M., and Kakihana, H. (1979) Raman spectra of polyborate ions in aqueous solution. *Journal of Inorganic and Nuclear Chemistry*, *41*, 1217-1220.

Manghnani, M.H., Hushur, A., Sekine, T., Wu, J., Stebbins, J.F. and Williams, Q. (2011) Raman, Brillouin and nuclear magnetic resonance spectroscopic studies on shocked borosilicate glass. *Journal of Applied Physics, 109,* 113509.

Mao, H.K., Xu, J.A., and Bell, P. M. (1986). Calibration of the ruby pressure gauge to 800 kbar under quasi-hydrostatic conditions. *Journal of Geophysical Research: Solid Earth*, *91*, 4673-4676.

Maya, L. (1976) Identification of polyborate and fluoropolyborate ions in solution by Raman spectroscopy. *Inorganic Chemistry*, *15*, 2179-2184.

Menzel, H., Schulz, H., and Deckert, H. (1935) Bildungs-und Existenzbedingungen des Kernits $Na_2B_4O_7{\cdot}4H_2O$. *Naturwissenschaften*, *23*, 832-833.

Menzel, H., and Schulz, H. (1940) Zur Kenntnis der Borsäuren und borsauren Alkalisalze. X. Der Kernit (Rasorit) $Na_2B_4O_7 \cdot 4H_2O$. *Zeitschrift fur Anorganische und Allgemeine Chemie*, *245*, 157-220.

Merlini, M., Cerantola, V., Gatta, G. D., Gemmi, M., Hanfland, M., Kupenko, I., Lotti, P., Muller, H., and Zhang, L. (2017). Dolomite-IV: Candidate structure for a carbonate in the Earth's lower mantle. *American Mineralogist, 102,* 1763-1766.

O'Bannon, E., and Williams, Q. (2014) Trona at extreme conditions: A pollutant sequestering material at high pressures and low temperatures. *American Mineralogist, 99,* 1973-1984.

O'Bannon, E., & Williams, Q. (2016) Beryl-II, a high-pressure phase of beryl: Raman and luminescence spectroscopy to 16.4 GPa. *Physics and Chemistry of Minerals*, *43*, 671-687.

Oganov, A.R., Ono, S., Ma, Y.M., Glass, C.W., and Garcia, A. (2008) Novel high-pressure structures of $MgCO_3$, $CaCO_3$ and CO_2 and their role in Earth's lower mantle. *Earth and Planetary Science Letters,* 273, 38–47.

Pabst, A., and Sawyer, D.L. (1948) Tincalconite crystals from Searles Lake, San Bernardino County, California. *American Mineralogist*, *33*, 472-481.

Pauling, L. (1960) The nature of the chemical bond and the structure of molecules and crystals: An introduction to modern structural chemistry. 3rd Edition, Cornell U. Press, Ithaca.

Always consult and cite the final, published document. See http:/www.minsocam.org or GeoscienceWorld

Ricardo, A., Carrigan, M.A., Olcott, A.N., and Benner, S.A. (2004) Borate minerals stabilize ribose. *Science*, *303*, 196-196.

Ross, V., and Edwards, J.D. (1959) On the crystal structure of kernite, $Na_2B_4O_7 \cdot 4H_2O$. *Acta Crystallographica* 12, 258-258.

Saladino, R., Barontini, M., Cossetti, C., Di Mauro, E., and Crestini, C. (2011) The effects of borate minerals on the synthesis of nucleic acid bases, amino acids and biogenic carboxylic acids from formamide. *Origins of Life and Evolution of Biospheres*, *41*, 317-330.

Sanjurjo, J. A., Lopez-Cruz, E., & Burns, G. (1983) High-pressure Raman study of zone-center phonons in $PbTiO_3$. *Physical Review B*, *28*, 7260.

Schaller, W.T. (1930) Borate minerals from the Kramer district, Mohave desert, California. *U.S. Geologic Survey Professional Paper* 158-I, 135-173.

Schubert, D.M. (2003) Borates in industrial use. In *Group 13 Chemistry III* (pp. 1-40). Springer Berlin Heidelberg.

Scorei, R. (2012) Is boron a prebiotic element? A mini-review of the essentiality of boron for the appearance of life on Earth. *Origins of Life and Evolution of Biospheres*, *42*, 3-17.

Scott, H.P., Liu, Z., Hemley, R.J. and Williams, Q. (2007) High-pressure infrared spectra of talc and lawsonite. *American Mineralogist, 92,* 1814-1820.

Sennova, N.A., et al. (2005) Room, low, and high temperature dehydration and phase transition of kernite in vacuum and in air. *Crystal Research and Technology,* 40, 563-572.

Shahar, A., Bassett, W.A., Mao, H.-K., Chou, I-M., and Mao, W. (2005) The stability and Raman spectra of ikaite, $CaCO_3 \cdot 6H_2O$, at high pressure and temperature, *American Mineralogist, 90,* 1835-1839.

Shannon, R.D. (1976) Revised effective ionic radii and systematic studies of interatomic distances in halides and chalcogenides*. Acta Crystallographica A, 32,* 751-767.

Smedskjaer, M.M., et al. (2014) Irreversibility of pressure induced boron speciation change in glass. *Scientific Reports, 4,* 3770.

Smith, W.C. (1968) Borax solution at Kramer, California. *Economic Geology*, *63*, 877-883.

Stephenson, J.D., Hallis, L.J., Nagashima, K., and Freeland, S.J. (2013) Boron enrichment in Martian clay. *PLOS One, 8,* e64624.

Takada, A., Catlow, C.R.A., and Price, G.D. (1995) Computer modeling of B_2O_3: Part I. New interatomic potentials, crystalline phases and predicted polymorphs, *Journal of Physics Condensed Matter, 7,* 8659-8692.

Always consult and cite the final, published document. See http:/www.minsocam.org or GeoscienceWorld

Thompson, E.C., Campbell, A. J., and Liu, Z. (2016) In-situ infrared spectroscopic studies of hydroxyl in amphiboles at high pressure. *American Mineralogist*, *101*, 706-712.

Vennari, C.E., and Williams, Q. (2018) A novel carbon bonding environment in deep mantle high-pressure dolomite. *American Mineralogist*, *103*, 171-174.

Vlasova, E.V., and Valyashko, M.G. (1966) Infrared absorption spectra of hydrated borates. *Russian Journal of Inorganic Chemistry*, *11*, 822-828.

Weir, C.E. (1966). Infrared spectra of the hydrated borates. *Journal of Research of the National Bureau of Standards. A*, *70*, 153-164.

Williams, Q., Jeanloz, R. and McMillan, P. (1987) Vibrational spectra of $MgSiO_3$-perovskite: Zero pressure Raman and mid-infrared spectra to 27 GPa. *Journal of Geophysical Research, 92*, 8116-8128.

Wondraczek, L., Sen, S., Behrens, H. and Youngman, R.E. (2007) Structure-energy map of alkali borosilicate glasses: Effects of pressure and temperature. *Physical Review B, 76,* 014202.

Yano, T., Kunimine, N., Shibata, S., and Yamane, M. (2003) Structural investigation of sodium borate glasses and melts by Raman spectroscopy: I. Quantitative evaluation of structural units. *Journal of Non-Crystalline Solids*, *321*, 137-146.

Zallen, R. (1974) Pressure-Raman effects and vibrational scaling laws in molecular crystals: S_8 and As_2S_3. *Physical Review B, 9,* 4485-4496.

Always consult and cite the final, published document. See http:/www.minsocam.org or GeoscienceWorld

This is a preprint, the final version is subject to change, of the American Mineralogist (MSA)
Cite as Authors (Year) Title. American Mineralogist, in press.
DOI: https://doi.org/10.2138/am-2018-6253

826

827

828

829

Figure 1

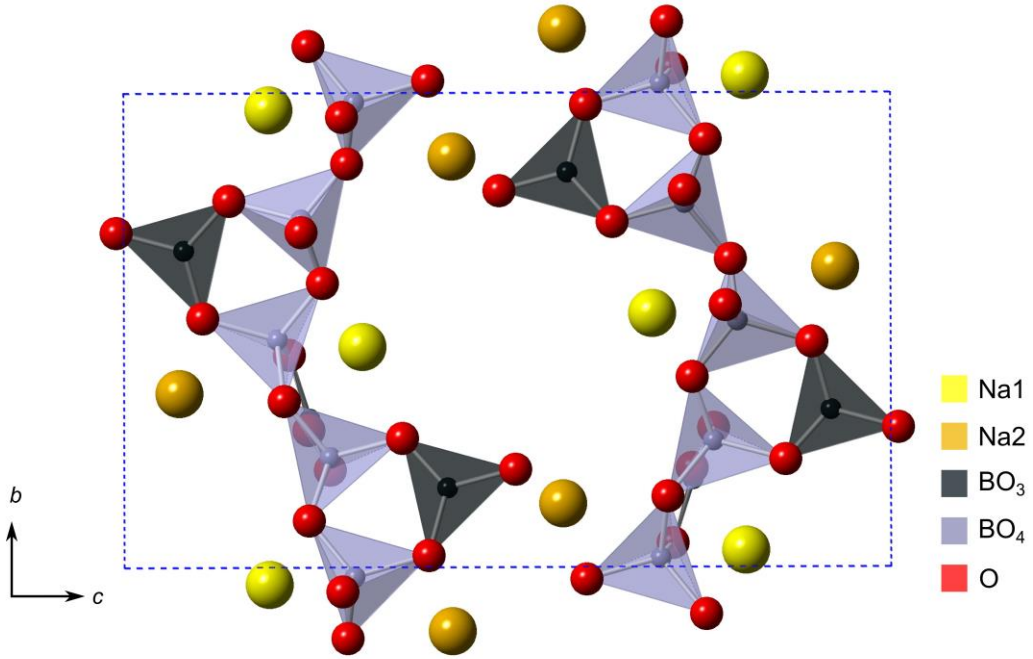

830

831 Figure 1. Crystal structure of kernite at room pressure and temperature. Crystal structure after
832 Cooper et al. (1973). Image generated in CrystalMaker ® software v.8.7.6.

833

Always consult and cite the final, published document. See http:/www.minsocam.org or GeoscienceWorld

This is a preprint, the final version is subject to change, of the American Mineralogist (MSA)
Cite as Authors (Year) Title. American Mineralogist, in press.
DOI: https://doi.org/10.2138/am-2018-6253

Figure 2

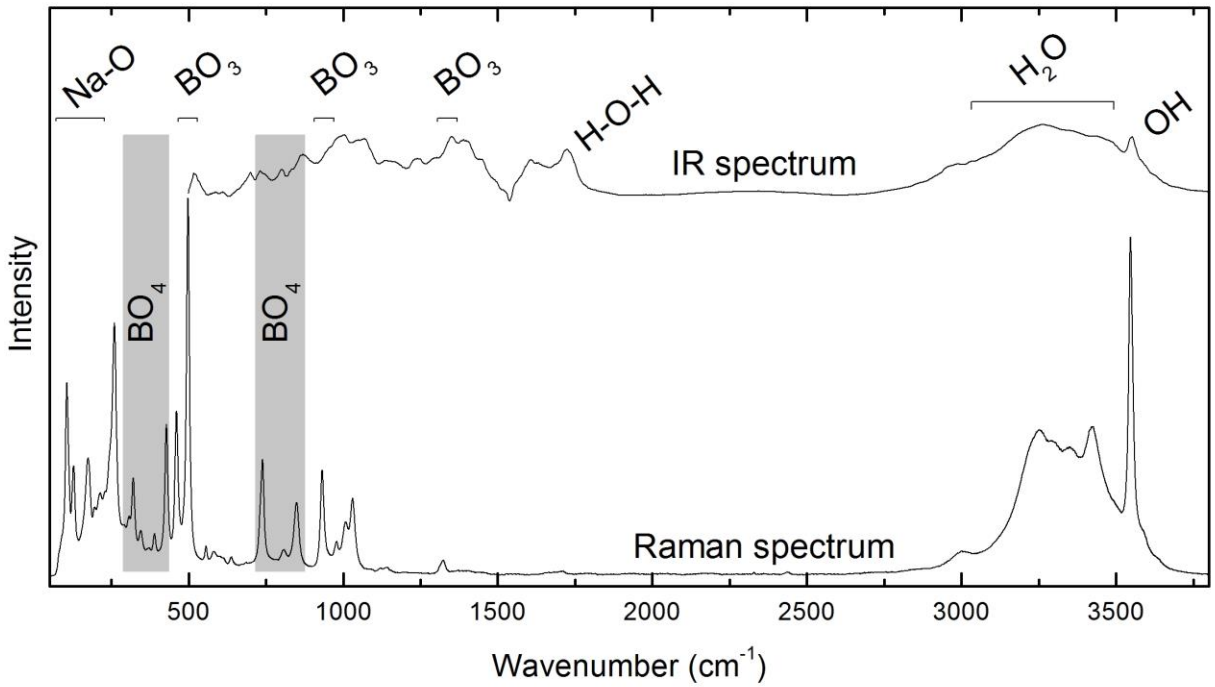

834
835 Figure 2. Ambient infrared and Raman spectrum of kernite.
836
837

Always consult and cite the final, published document. See http:/www.minsocam.org or GeoscienceWorld

Figure 3a

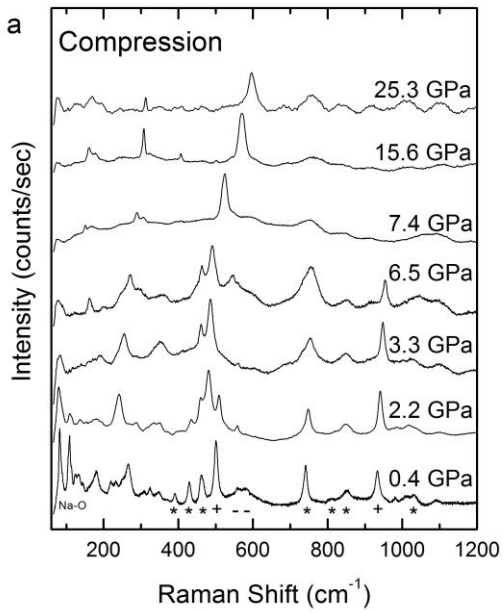

Figure 3b

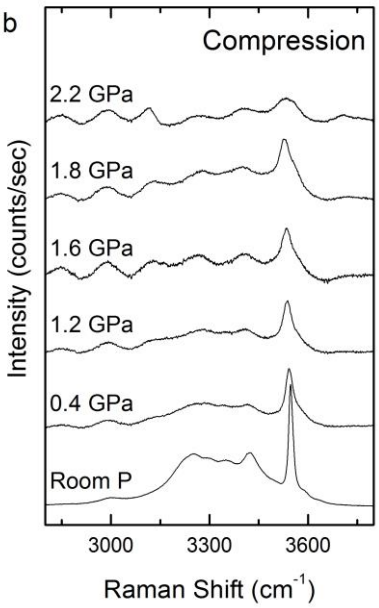

Figure 3. Representative Raman spectrum of kernite on compression (a) low frequency region (b) OH stretching region. Note the dramatic change in the Raman spectrum under compression. Modulation in the OH stretching region is an artifact. Modes are labeled below the 0.4 GPa spectrum, * BO_4 modes, + BO_3 modes, and - OH Libration.

Always consult and cite the final, published document. See http:/www.minsocam.org or GeoscienceWorld

846

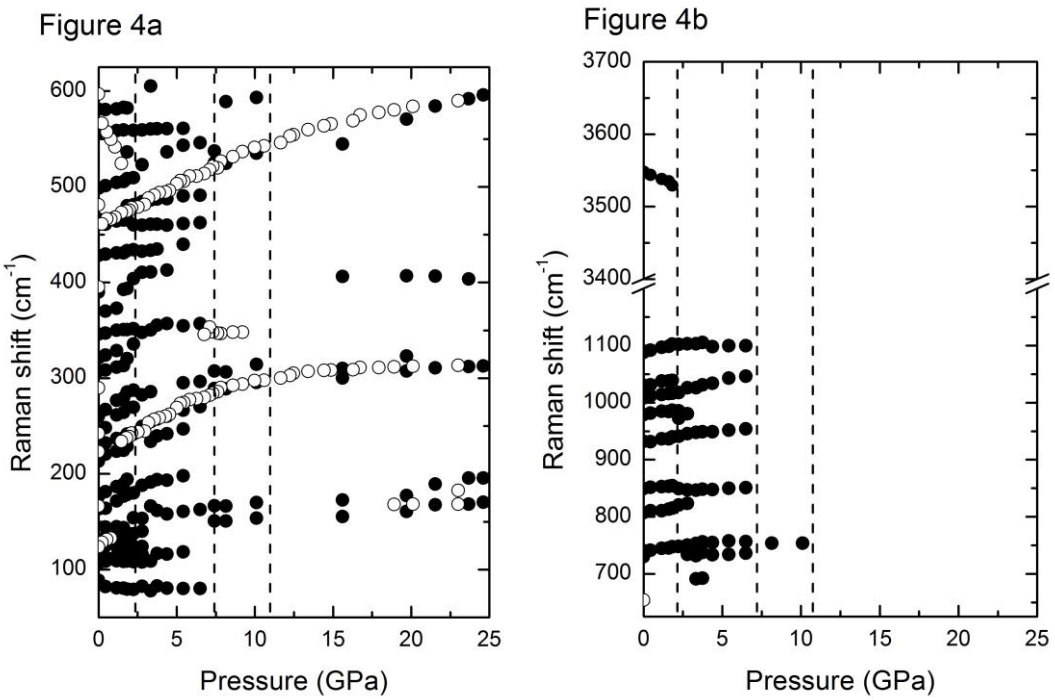

847

848 Figure 4. Raman mode shifts of kernite up to ~25 GPa (a) 50 - 625 cm^{-1} and (b) 650 - 3700 cm^{-1}.
849 Closed circles are compression and open circles are decompression and error bars are smaller
850 than the symbols. Vertical dashed lines indicate phase transition pressures. Note that very few
851 modes return on decompression, and that most return only after the sample is fully
852 decompressed to room pressure.

853

Always consult and cite the final, published document. See http:/www.minsocam.org or GeoscienceWorld

Figure 5

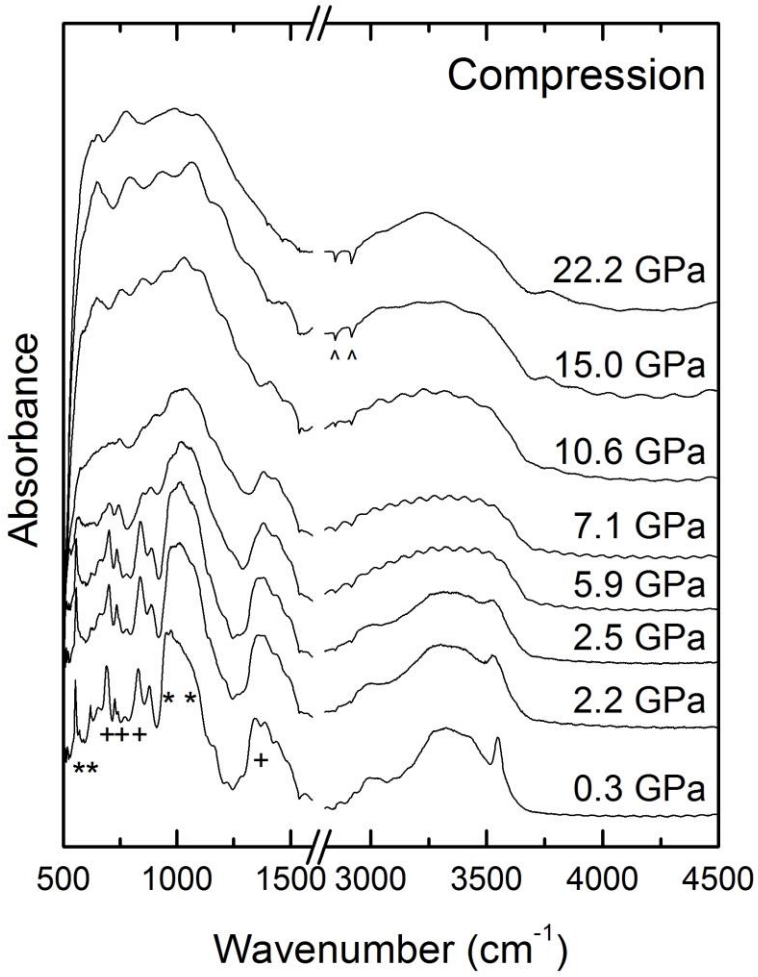

Figure 5. Representative high-pressure infrared spectra of kernite up to ~22.2 GPa. Fringing in the OH region of several infrared spectra is an artifact. Modes are labeled below the 0.4 GPa spectrum, * BO_4 modes, + BO_3 modes, and - OH Libration. ^ are due to hydrocarbon contamination.

Always consult and cite the final, published document. See http:/www.minsocam.org or GeoscienceWorld

This is a preprint, the final version is subject to change, of the American Mineralogist (MSA)
Cite as Authors (Year) Title. American Mineralogist, in press.
DOI: https://doi.org/10.2138/am-2018-6253

861

Figure 6

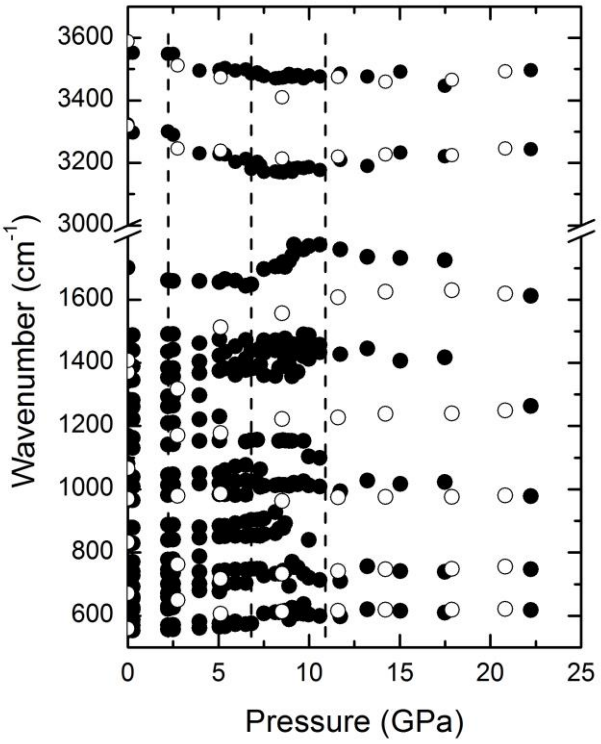

862

863 Figure 6. Infrared mode shifts of kernite up to ~23 GPa. Closed circles are compression and
864 open circles are decompression and error bars are smaller than the symbols. Vertical dashed
865 lines indicate phase transition pressures.

866

Always consult and cite the final, published document. See http:/www.minsocam.org or GeoscienceWorld

867

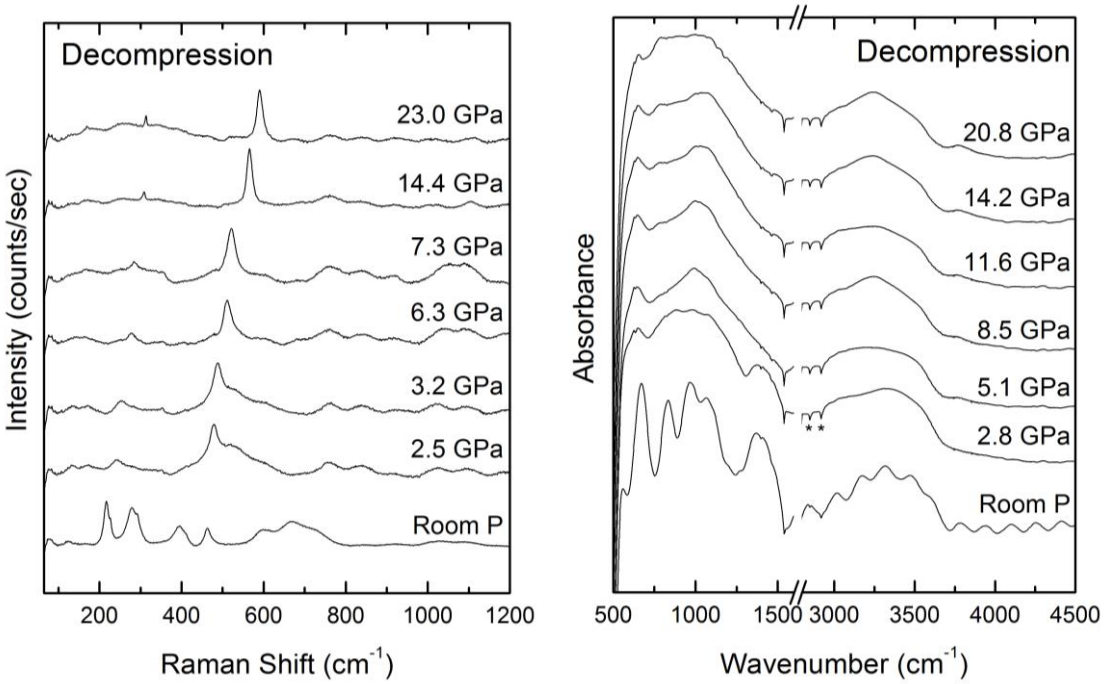

868
869

870 Figure 7 Decompression spectra of kernite (a) Raman and (b) infrared. Fringing in the OH region
871 in the room pressure infrared spectrum is an artifact.
872

873
874

Always consult and cite the final, published document. See http:/www.minsocam.org or GeoscienceWorld

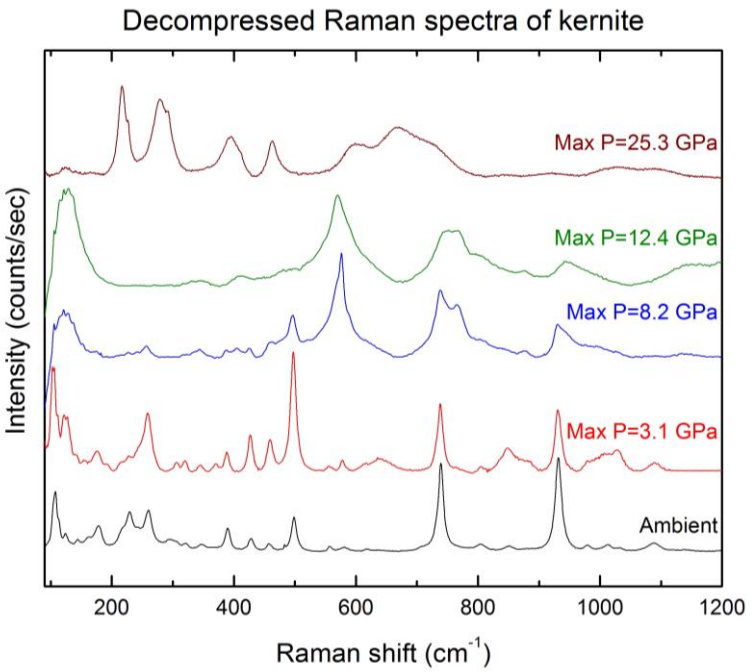

Figure 8. Decompressed Raman spectra of kernite compressed to pressures just above each proposed phase transition. Note the ~2.5 GPa transition is fully reversible, and that the ~7.0 GPa transition is partially reversible. Above 12.4 GPa the decompressed spectra are not like the starting spectrum.

Always consult and cite the final, published document. See http:/www.minsocam.org or GeoscienceWorld

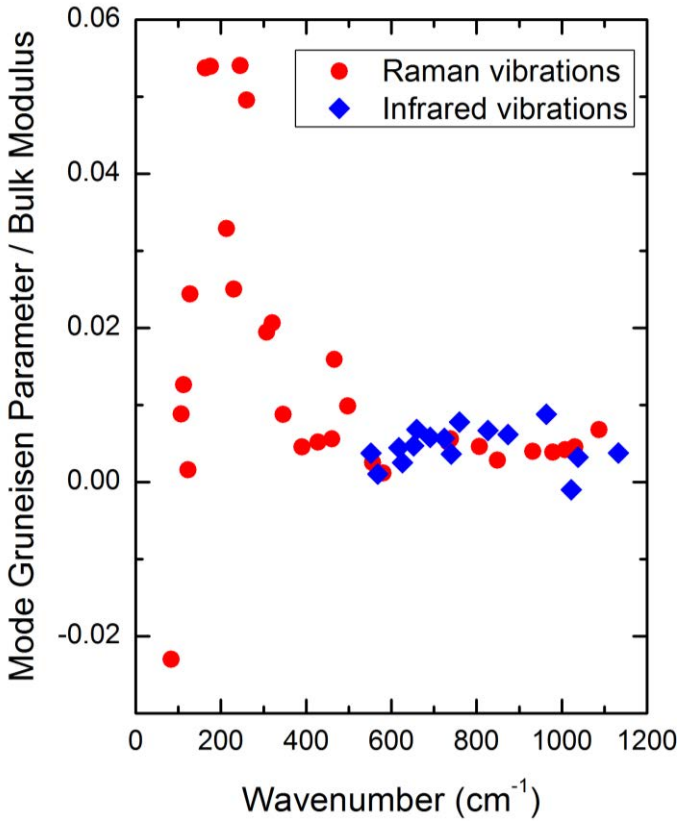

Figure 9. Trend of normalized mode shifts versus frequency for the low-pressure phase of kernite. Normalized mode shifts are calculated from 1/ω(dω/dP) (which is equivalent to the mode Gruneisen parameter divided by the bulk modulus).

Always consult and cite the final, published document. See http:/www.minsocam.org or GeoscienceWorld

This is a preprint, the final version is subject to change, of the American Mineralogist (MSA)
Cite as Authors (Year) Title. American Mineralogist, in press.
DOI: https://doi.org/10.2138/am-2018-6253

ν_{0i} (cm^{-1})	Assignment	($d\nu_{0i}/dP$) to 2.5GPa (cm^{-1}/GPa)
83*	Na-O	-1.91 (±0.27)
107	Na-O	0.94 (±0.47)
113	Na-O	1.42 (±0.14)
123	Na-O	0.20 (±0.39)
128	Na-O	3.13 (±1.26)
163		8.78 (±0.88)
175		9.46 (±0.31)
214		7.02 (±1.38)
230		5.76 (±0.75)
246		13.28 (±1.28)
260		12.90 (±1.04)
308		5.98 (±1.80)
321		6.63 (±0.20)
346		3.05 (±0.12)
390	δ BO_4	1.79 (±0.18)
428	BO_4	2.23 (±0.43)
461	BO_4	2.58 (±0.11)
466	δ BO_3	7.43 (±1.24)
498	δ BO_3	4.92 (±0.54)
557	O-H Libration	1.41 (±0.31)
581	O-H Libration	0.69 (±0.43)
733	ν_s BO_4	3.82 (±0.49)
739	ν_s BO_4	4.16 (±0.37)
807	ν_s BO_4	3.73 (±0.72)
850	ν_s BO_4	2.42 (±0.39)
932	ν_s BO_3	3.73 (±0.64)
979		3.80 (±0.73)
1008		4.23 (±0.54)
1031	ν_{as} BO_4	4.69 (±0.71)
1088		7.41 (±0.81)
3004	H_2O	-
3255	H_2O	-
3301	H_2O	-
3351	H_2O	-
3425	H_2O	-
3548	OH stretch	-9.20 (±1.05)

Table 1. Observed room pressure and temperature Raman modes of kernite. Assignments after Klopproge and Frost (1999).
*Modes extrapolated to room pressure
ν_s symmetric stretch, ν_{as} antisymmetric stretch, δ bend

Always consult and cite the final, published document. See http:/www.minsocam.org or GeoscienceWorld

ν_{0i} (cm^{-1})	Assignment	($d\nu_{0i}/dP$) to 2.5 GPa (cm^{-1}/GPa)
552.3	BO_4	2.07 (±0.17)
568.4	BO_4	0.60 (±0.38)
618.0	δ BO_3	2.77 (±0.76)
626.3*		1.58 (±0.17)
652.7	δ BO_3	3.09 (±0.19)
659.7*		4.50 (±0.95)
691.2	δ BO_3	4.04 (±0.11)
724.5		4.14 (±0.38)
740.8		2.70 (±0.37)
760.1	ν_s BO_4	5.94 (±2.05)
826.7	ν_s BO_4	5.56 (±0.26)
874.1	ν_s BO_3	5.42 (±0.59)
963.6	ν_{as} BO_4	8.51 (±0.47)
1022.1	ν_{as} BO_4	-1.02 (±2.90)
1038.2*		3.38 (±0.75)
1132.7		4.28 (±0.62)
1260.5*		1.33 (±0.88)
1284.4		4.25 (±0.81)
1341.6	ν_{as} BO_3	5.15 (±0.44)
1387.8		-2.24 (±0.50)
1434.0		1.05 (±1.86)
1486.9		1.80 (±0.33)
1701.9	δ H-O-H	-17.58 (±0.67)
3323.2	H_2O	-7.78 (±5.67)
3551.4	OH	-13.63 (±2.20)

Table 2. Observed room pressure and temperature infrared modes of kernite. Assignments after Jun et al. (1995).
ν_s symmetric stretch, ν_{as} antisymmetric stretch, δ bend
*Modes extrapolated to room pressure

Always consult and cite the final, published document. See http:/www.minsocam.org or GeoscienceWorld

ν_{0i} (cm^{-1})	Assignment	Raman (R) Infrared (IR)
124.0	Na-O	R
168.2	Na-O	R
217.3		R
226.1 sh		R
279.3		R
290.8 sh		R
395.3		R
410.3 sh		R
462.5	δ BO_3 & BO_4	R
598.3	δ BO_3 & BO_4	R
667.1		R
672.0		IR
735.5	ν_s BO_4	R
833.5	ν_s BO_4	IR
971.0	ν_{as} BO_4	IR
1073.9	ν_{as} BO_4?	IR
1127.8 sh	ν_{as} BO_4	IR
1198.9		IR
1272.4		IR
1368.0	ν_{as} BO_3	IR
1477.6		IR

Table 3. Observed Raman and infrared frequencies of decompressed product from 25.3 GPa. sh shoulder, ν_s symmetric stretch, ν_{as} antisymmetric stretch, δ bend

Always consult and cite the final, published document. See http:/www.minsocam.org or GeoscienceWorld

This is a preprint, the final version is subject to change, of the American Mineralogist (MSA)
Cite as Authors (Year) Title. American Mineralogist, in press.
DOI: https://doi.org/10.2138/am-2018-6253

Figure 1

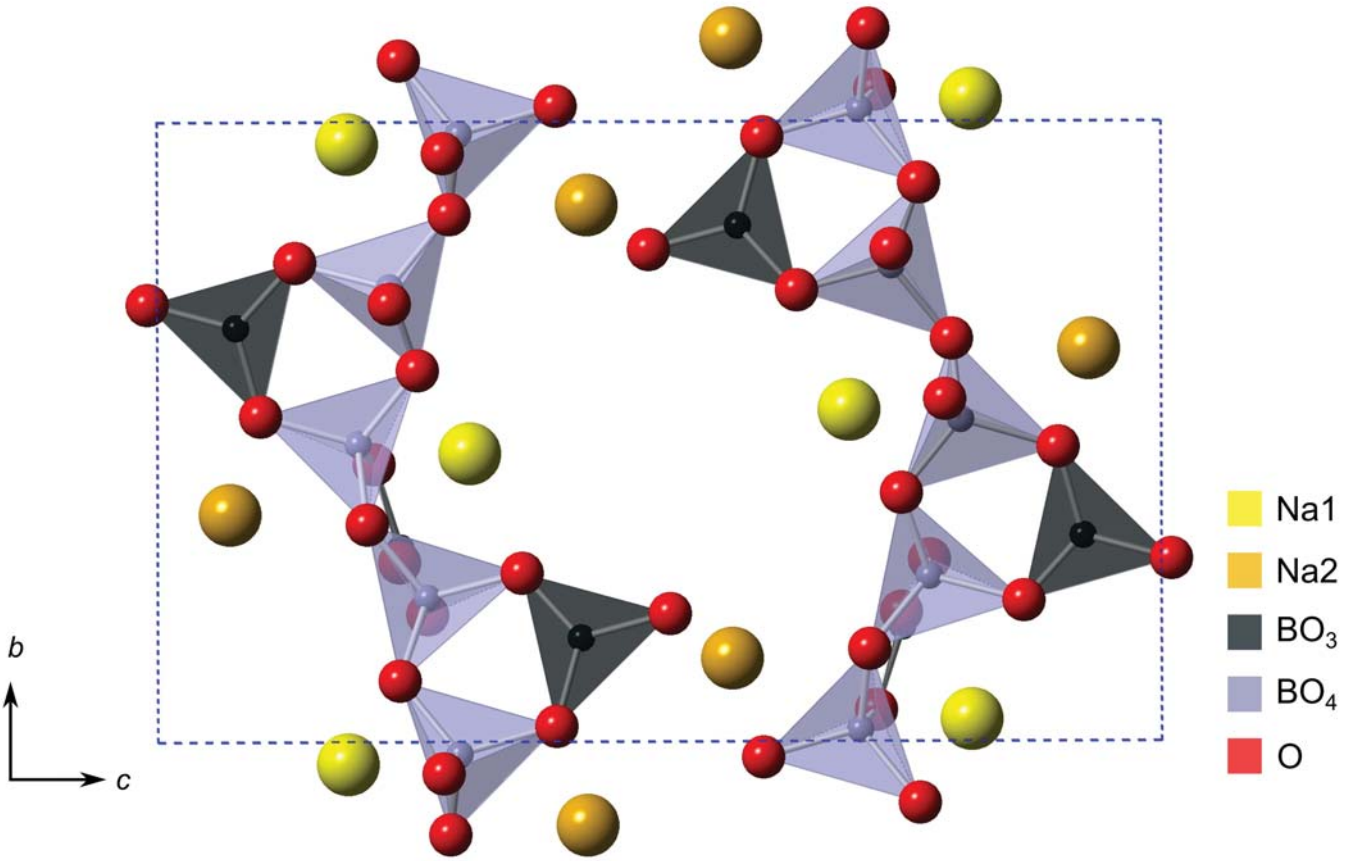

Always consult and cite the final, published document. See http:/www.minsocam.org or GeoscienceWorld

This is a preprint, the final version is subject to change, of the American Mineralogist (MSA)
Cite as Authors (Year) Title. American Mineralogist, in press.
DOI: https://doi.org/10.2138/am-2018-6253

Figure 2

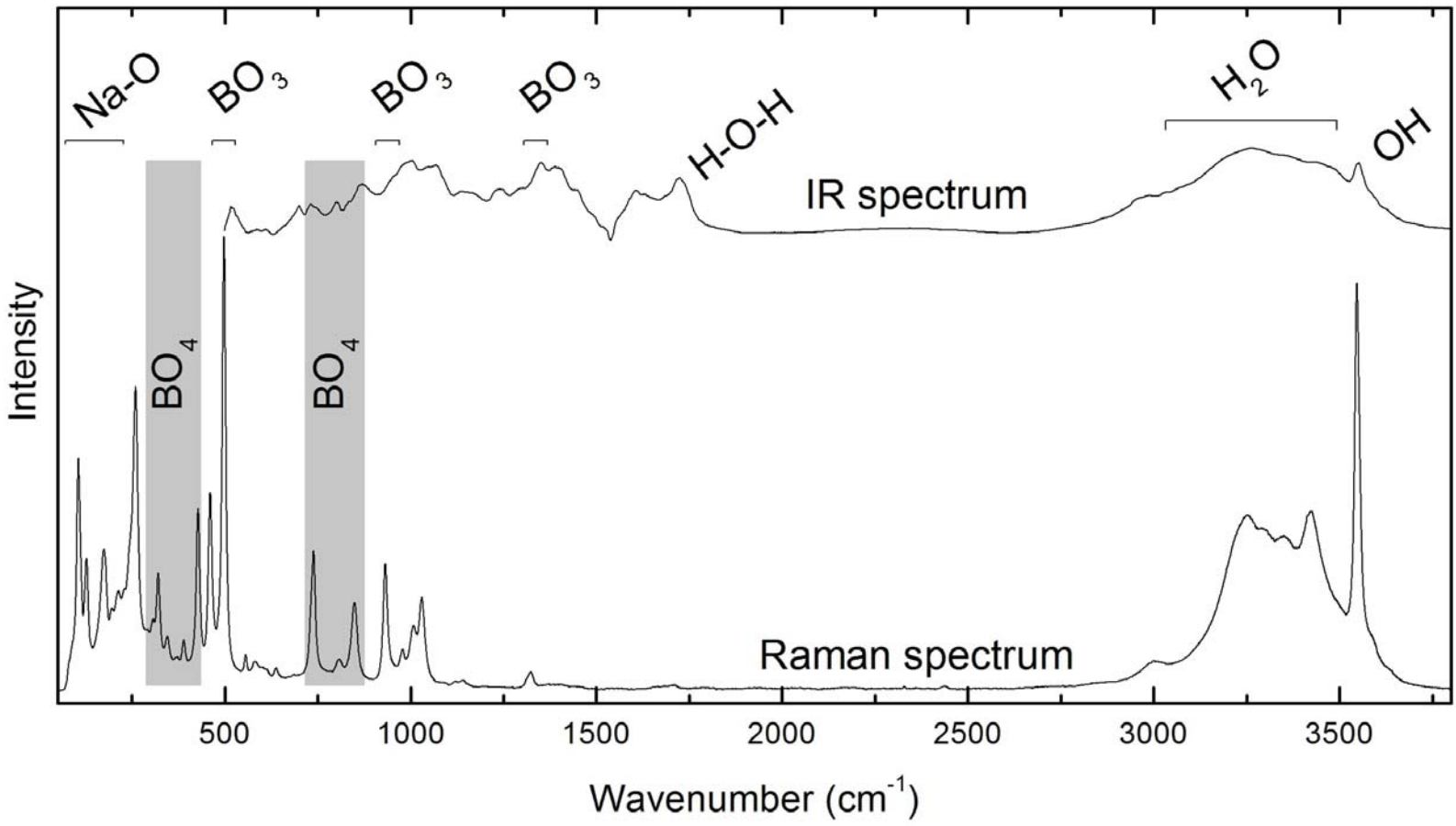

Always consult and cite the final, published document. See http:/www.minsocam.org or GeoscienceWorld

This is a preprint, the final version is subject to change, of the American Mineralogist (MSA)
Cite as Authors (Year) Title. American Mineralogist, in press.
DOI: https://doi.org/10.2138/am-2018-6253

Figure 3a

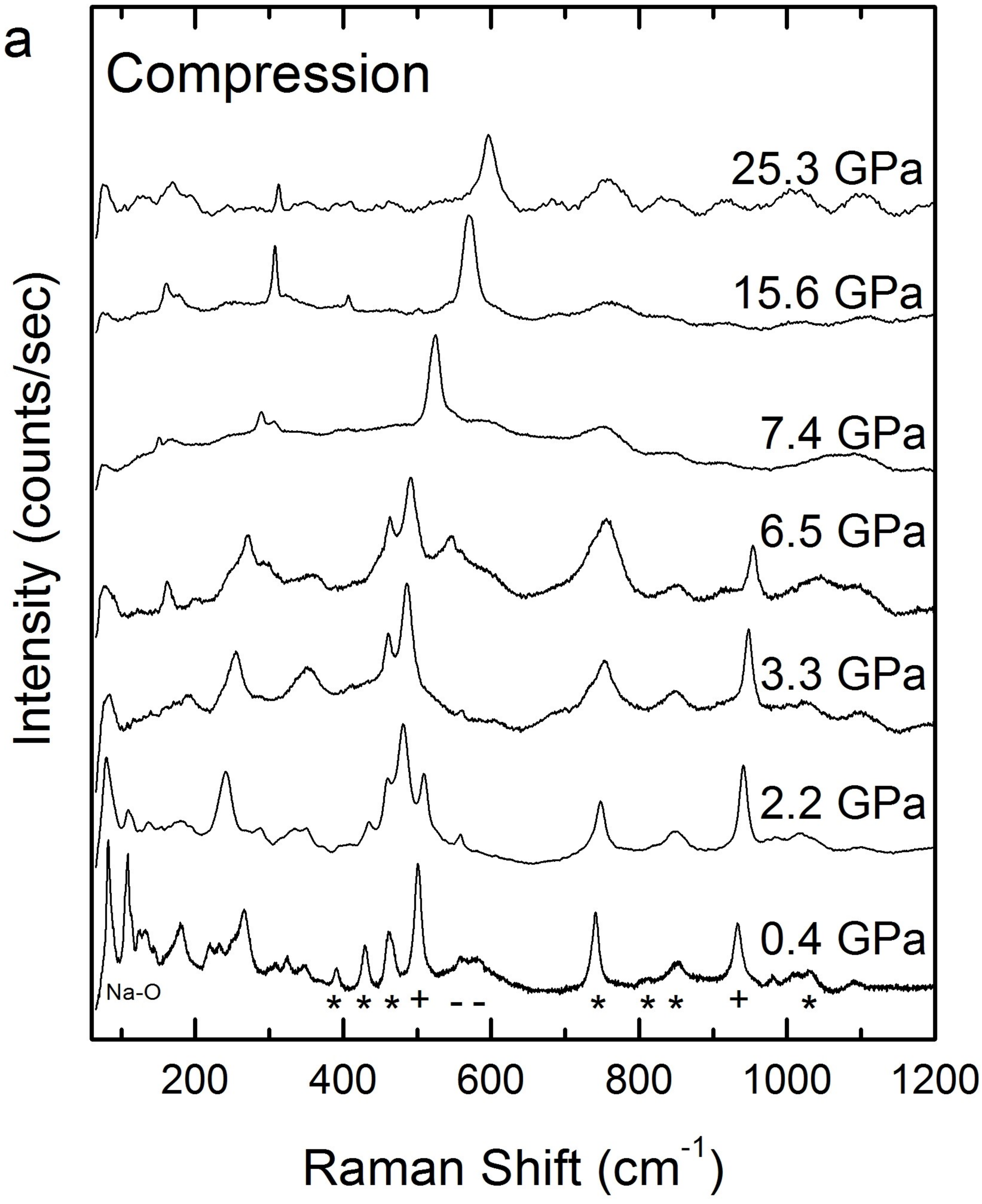

Always consult and cite the final, published document. See http:/www.minsocam.org or GeoscienceWorld

This is a preprint, the final version is subject to change, of the American Mineralogist (MSA)
Cite as Authors (Year) Title. American Mineralogist, in press.
DOI: https://doi.org/10.2138/am-2018-6253

Figure 3b

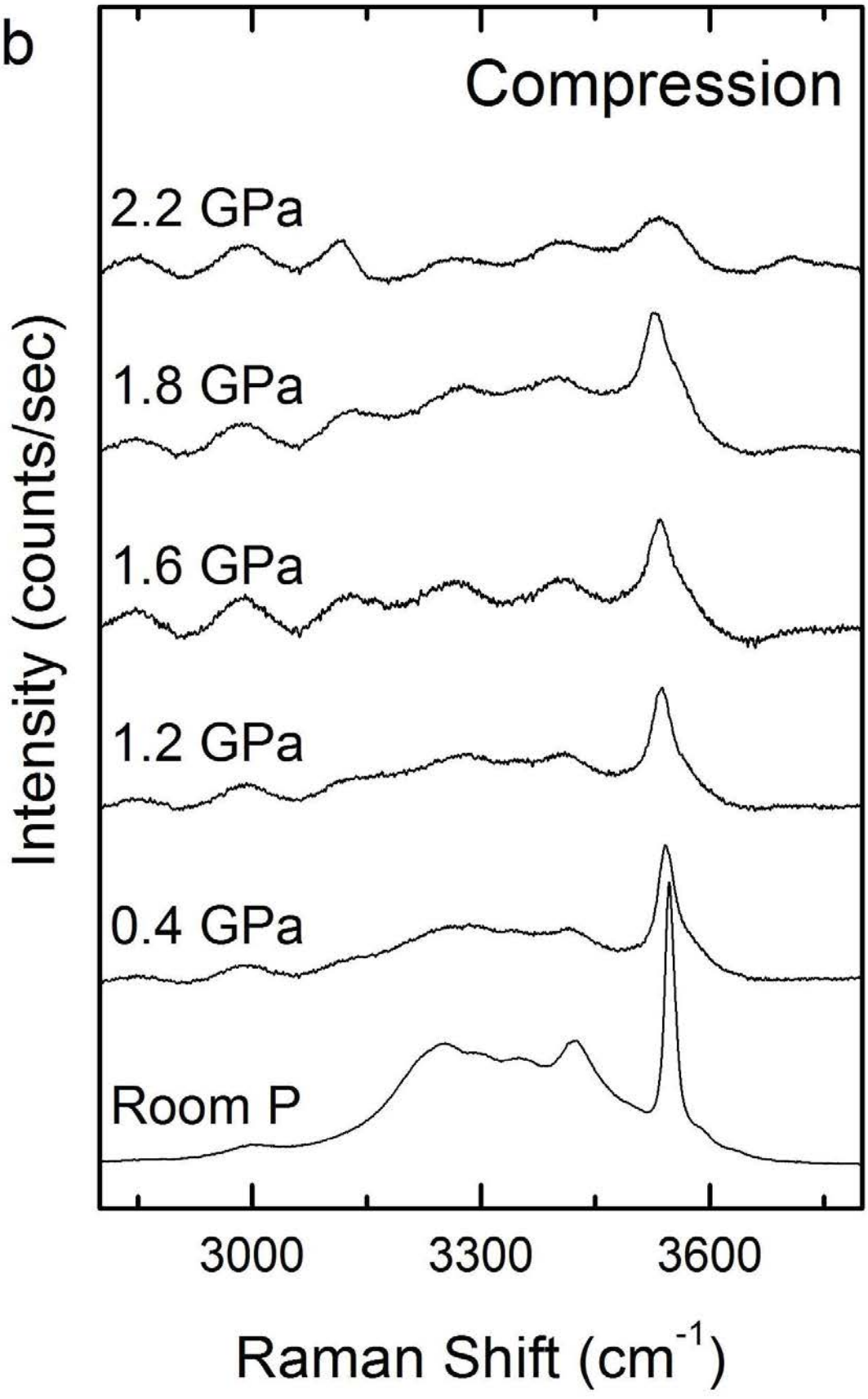

Always consult and cite the final, published document. See http:/www.minsocam.org or GeoscienceWorld

This is a preprint, the final version is subject to change, of the American Mineralogist (MSA)
Cite as Authors (Year) Title. American Mineralogist, in press.
DOI: https://doi.org/10.2138/am-2018-6253

Figure 4a

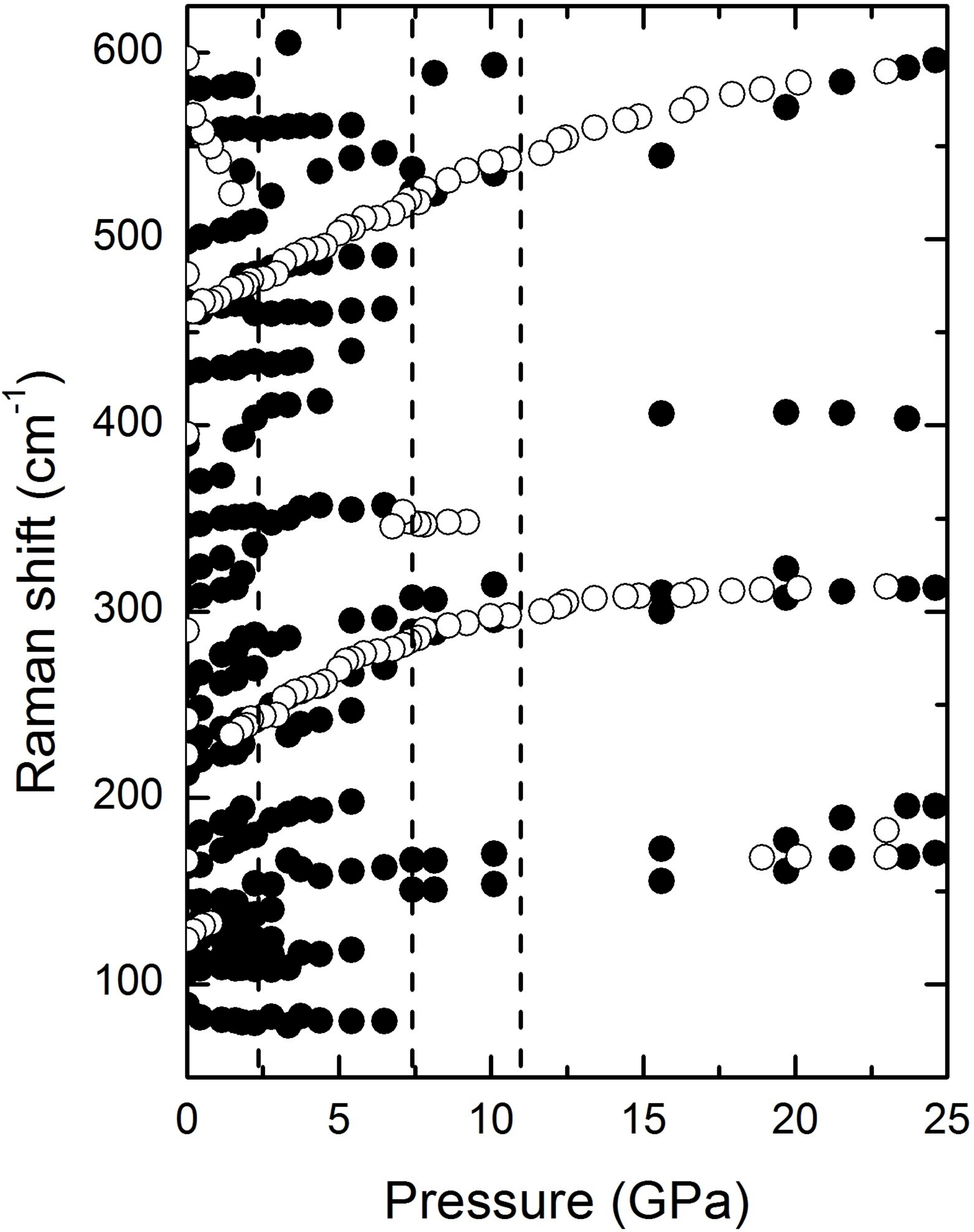

Always consult and cite the final, published document. See http:/www.minsocam.org or GeoscienceWorld

This is a preprint, the final version is subject to change, of the American Mineralogist (MSA)
Cite as Authors (Year) Title. American Mineralogist, in press.
DOI: https://doi.org/10.2138/am-2018-6253

Figure 4b

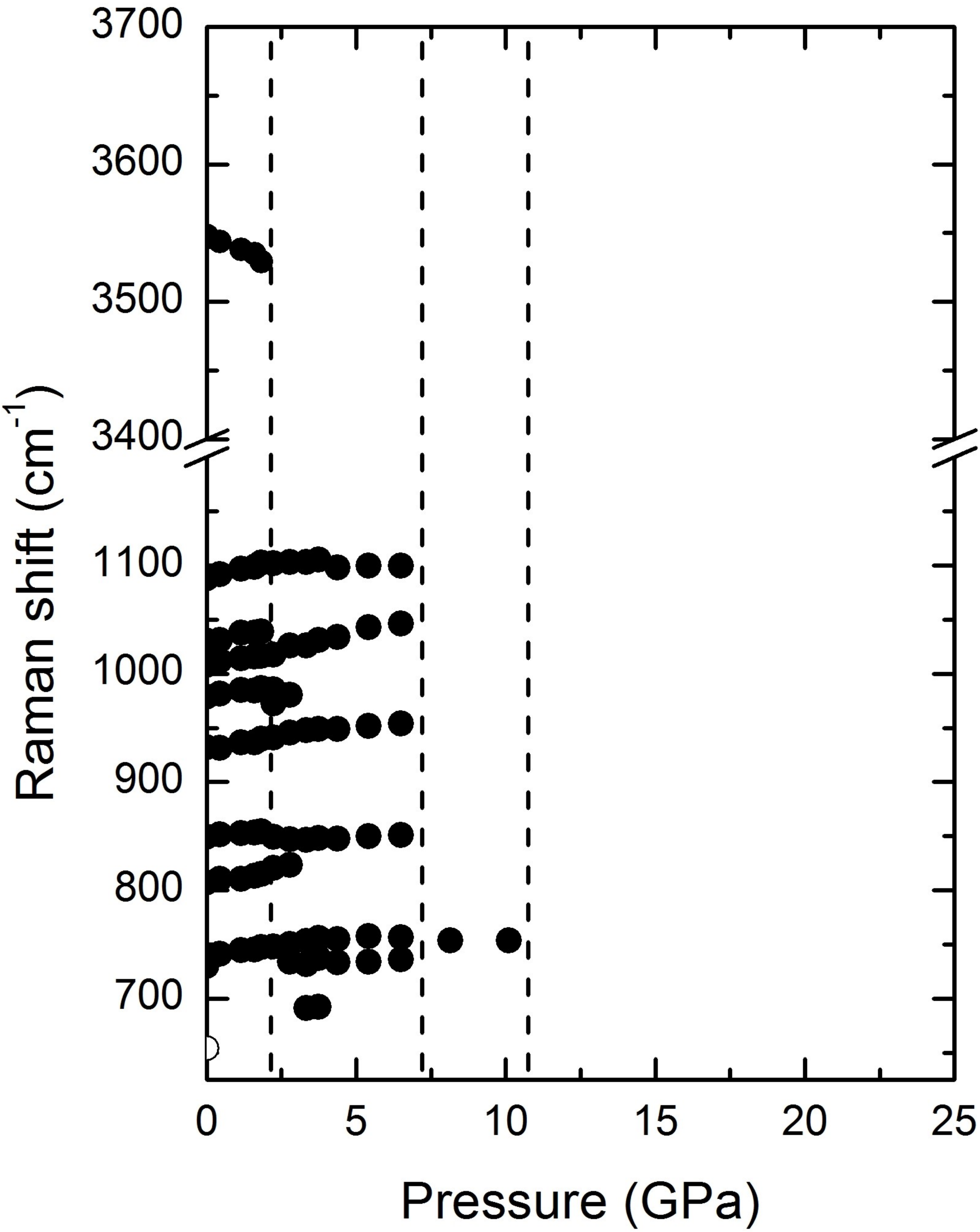

Always consult and cite the final, published document. See http:/www.minsocam.org or GeoscienceWorld

This is a preprint, the final version is subject to change, of the American Mineralogist (MSA)
Cite as Authors (Year) Title. American Mineralogist, in press.
DOI: https://doi.org/10.2138/am-2018-6253

Figure 5

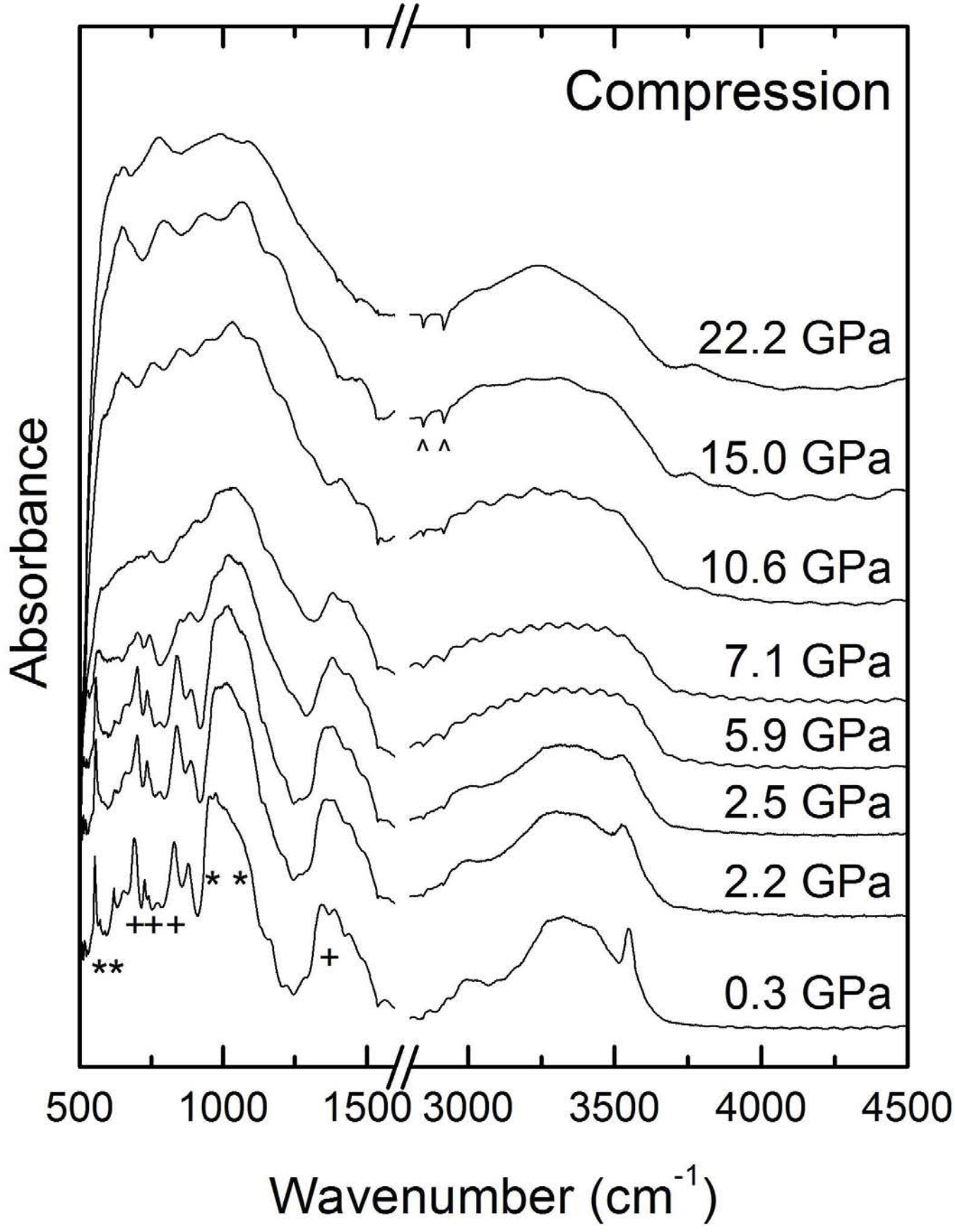

Always consult and cite the final, published document. See http:/www.minsocam.org or GeoscienceWorld

This is a preprint, the final version is subject to change, of the American Mineralogist (MSA)
Cite as Authors (Year) Title. American Mineralogist, in press.
DOI: https://doi.org/10.2138/am-2018-6253

Figure 6

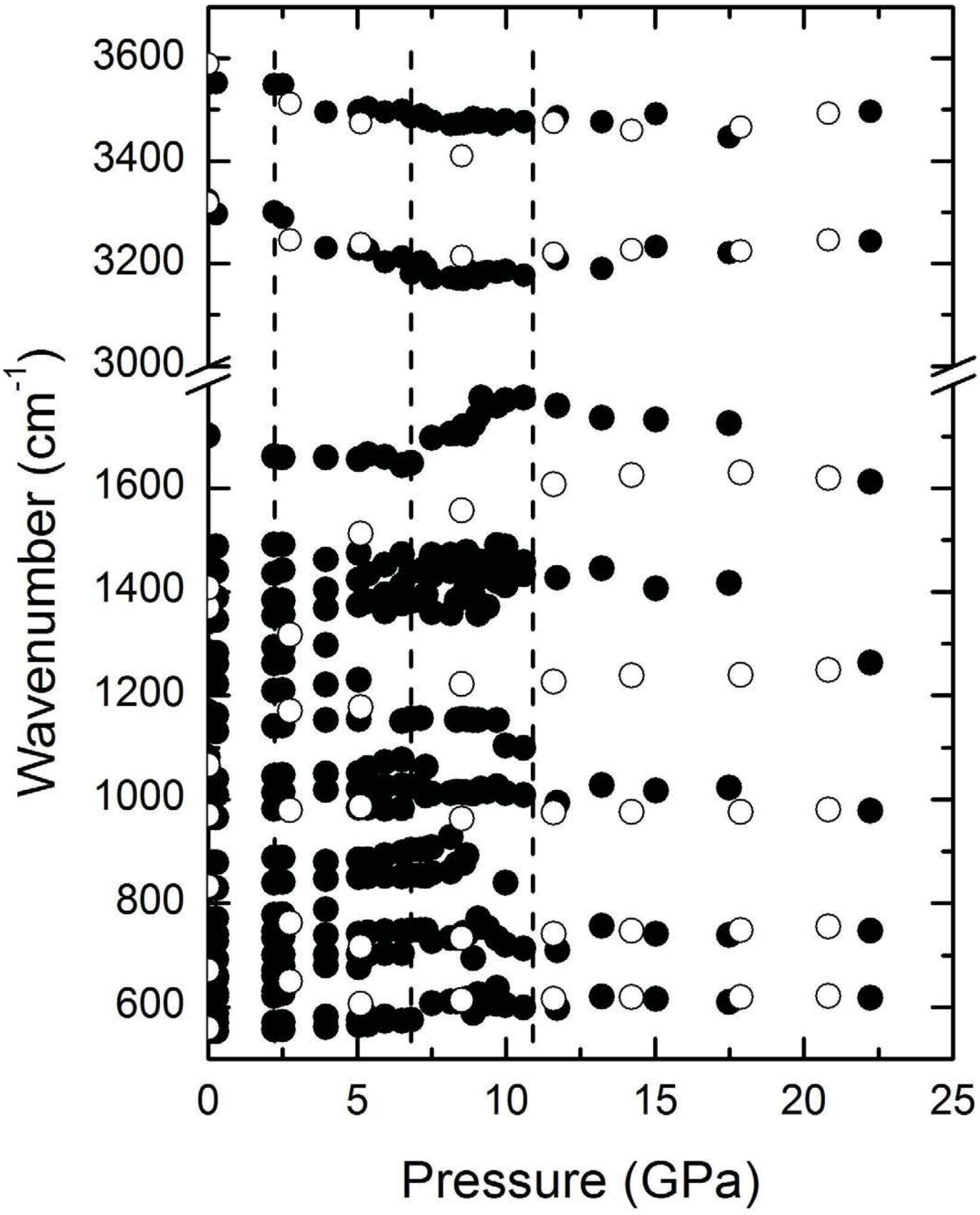

Always consult and cite the final, published document. See http:/www.minsocam.org or GeoscienceWorld

This is a preprint, the final version is subject to change, of the American Mineralogist (MSA)
Cite as Authors (Year) Title. American Mineralogist, in press.
DOI: https://doi.org/10.2138/am-2018-6253

Figure 7

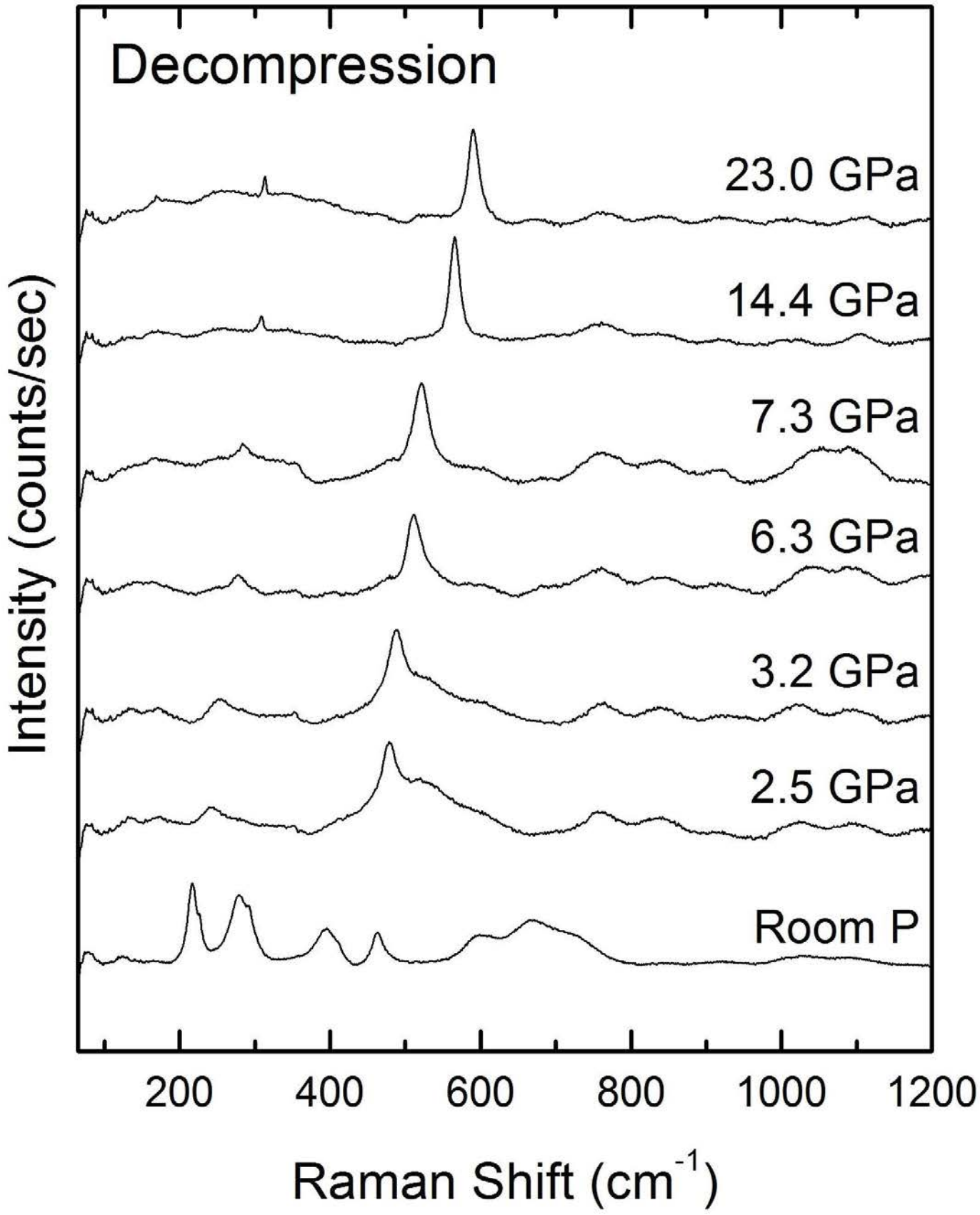

Always consult and cite the final, published document. See http:/www.minsocam.org or GeoscienceWorld

This is a preprint, the final version is subject to change, of the American Mineralogist (MSA)
Cite as Authors (Year) Title. American Mineralogist, in press.
DOI: https://doi.org/10.2138/am-2018-6253

Figure 8

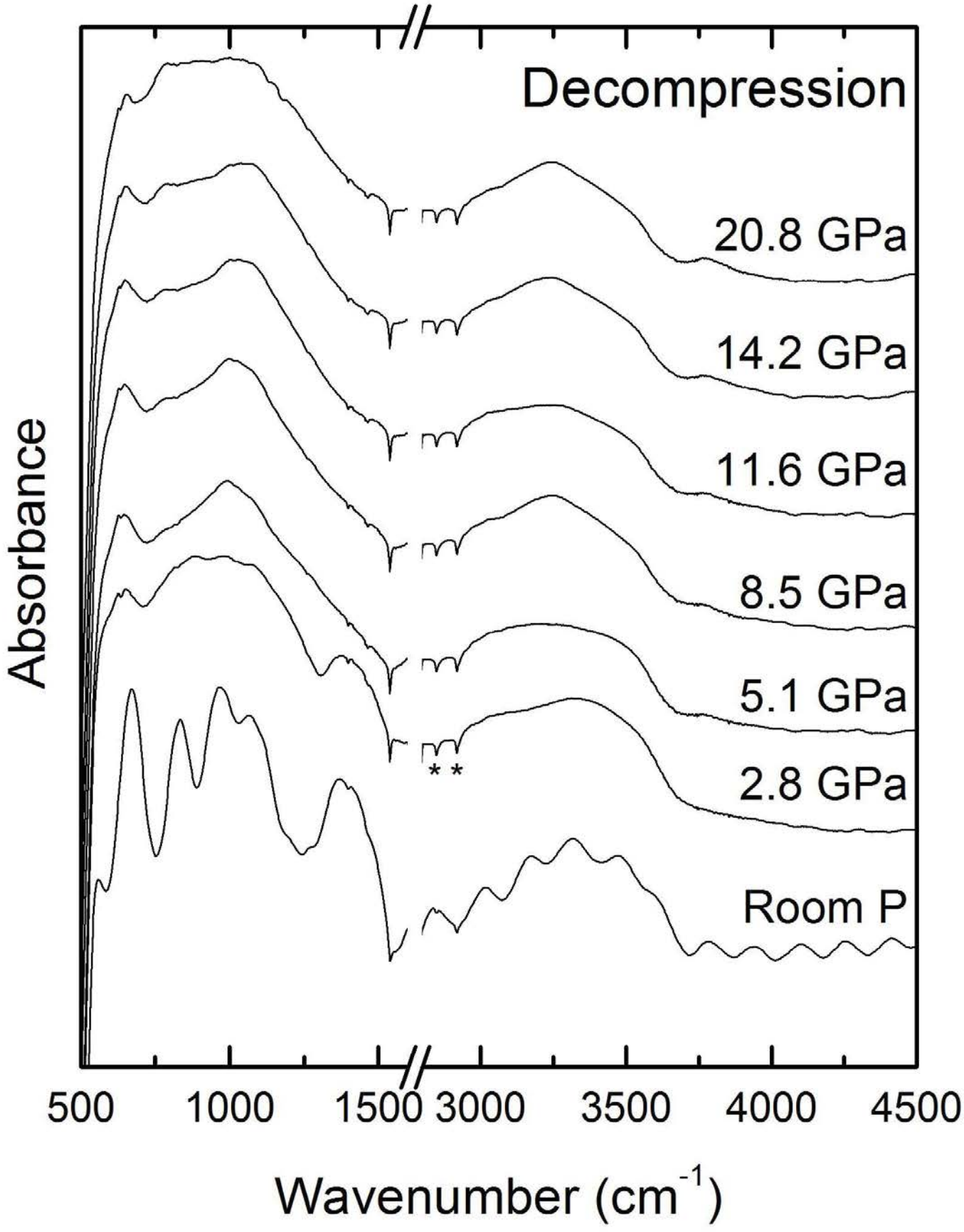

Always consult and cite the final, published document. See http:/www.minsocam.org or GeoscienceWorld

This is a preprint, the final version is subject to change, of the American Mineralogist (MSA)
Cite as Authors (Year) Title. American Mineralogist, in press.
DOI: https://doi.org/10.2138/am-2018-6253

Figure 9

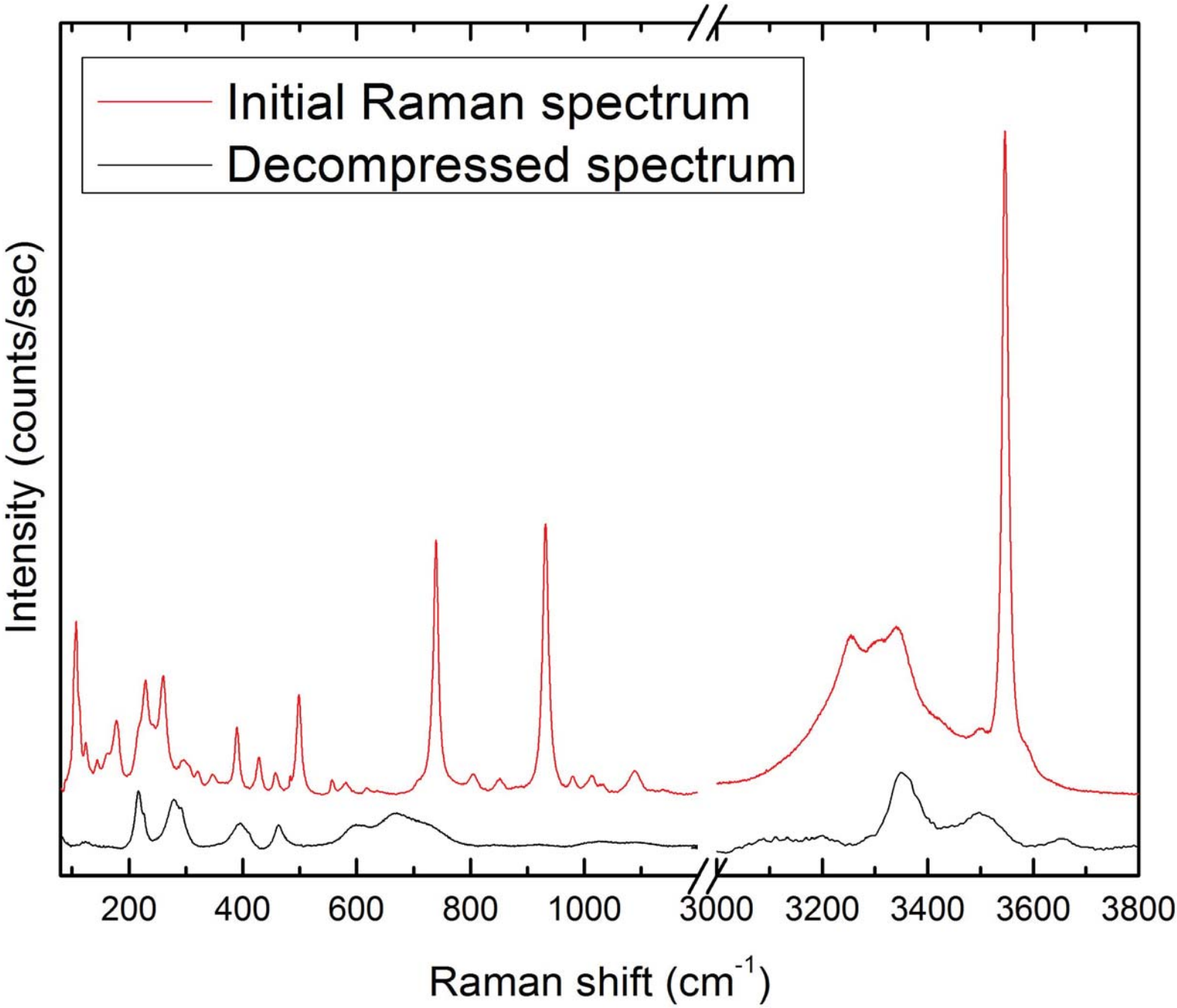

Always consult and cite the final, published document. See http:/www.minsocam.org or GeoscienceWorld

This is a preprint, the final version is subject to change, of the American Mineralogist (MSA)
Cite as Authors (Year) Title. American Mineralogist, in press.
DOI: https://doi.org/10.2138/am-2018-6253

Figure 10

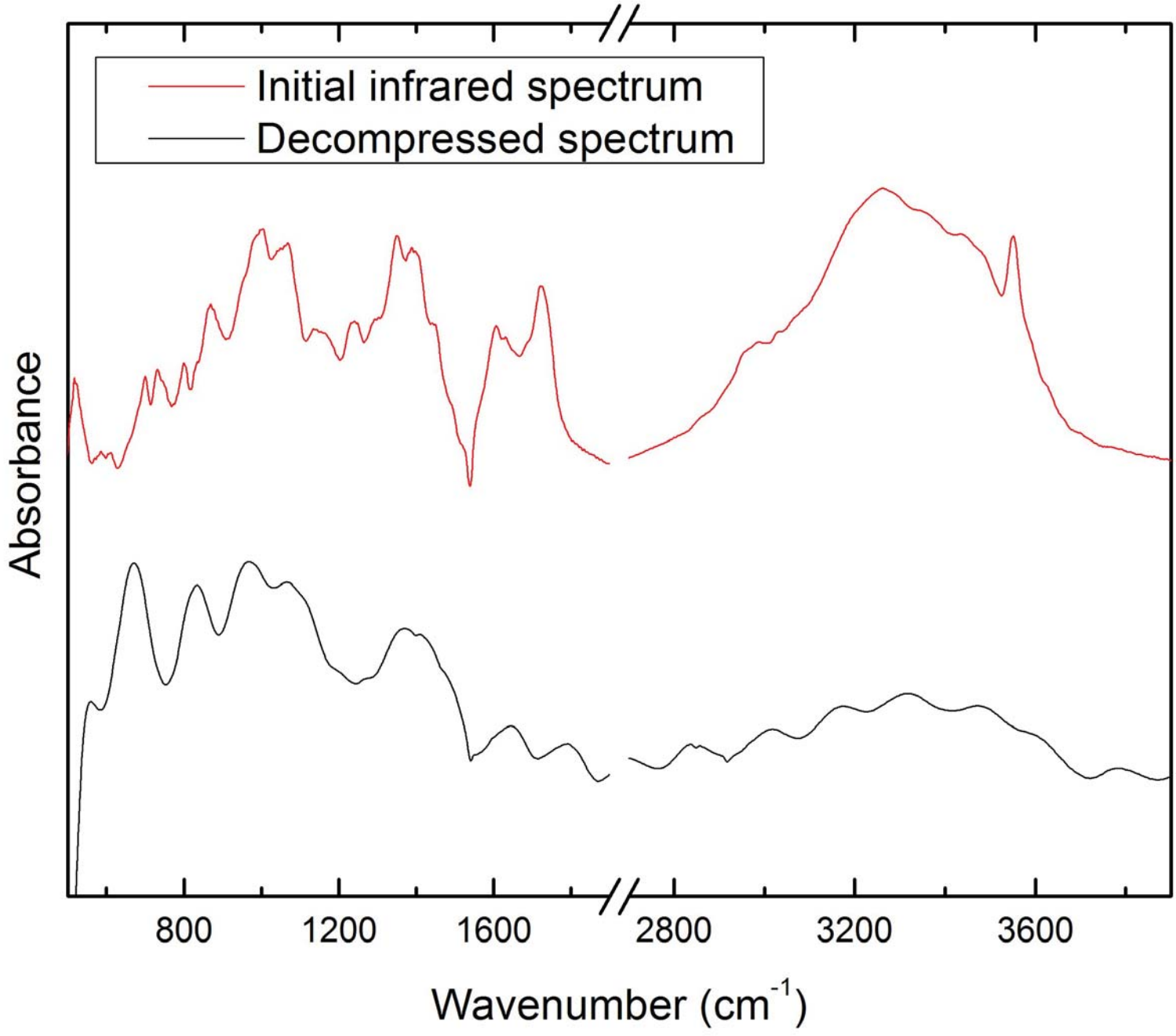

Always consult and cite the final, published document. See http:/www.minsocam.org or GeoscienceWorld

This is a preprint, the final version is subject to change, of the American Mineralogist (MSA)
Cite as Authors (Year) Title. American Mineralogist, in press.
DOI: https://doi.org/10.2138/am-2018-6253

Figure 11

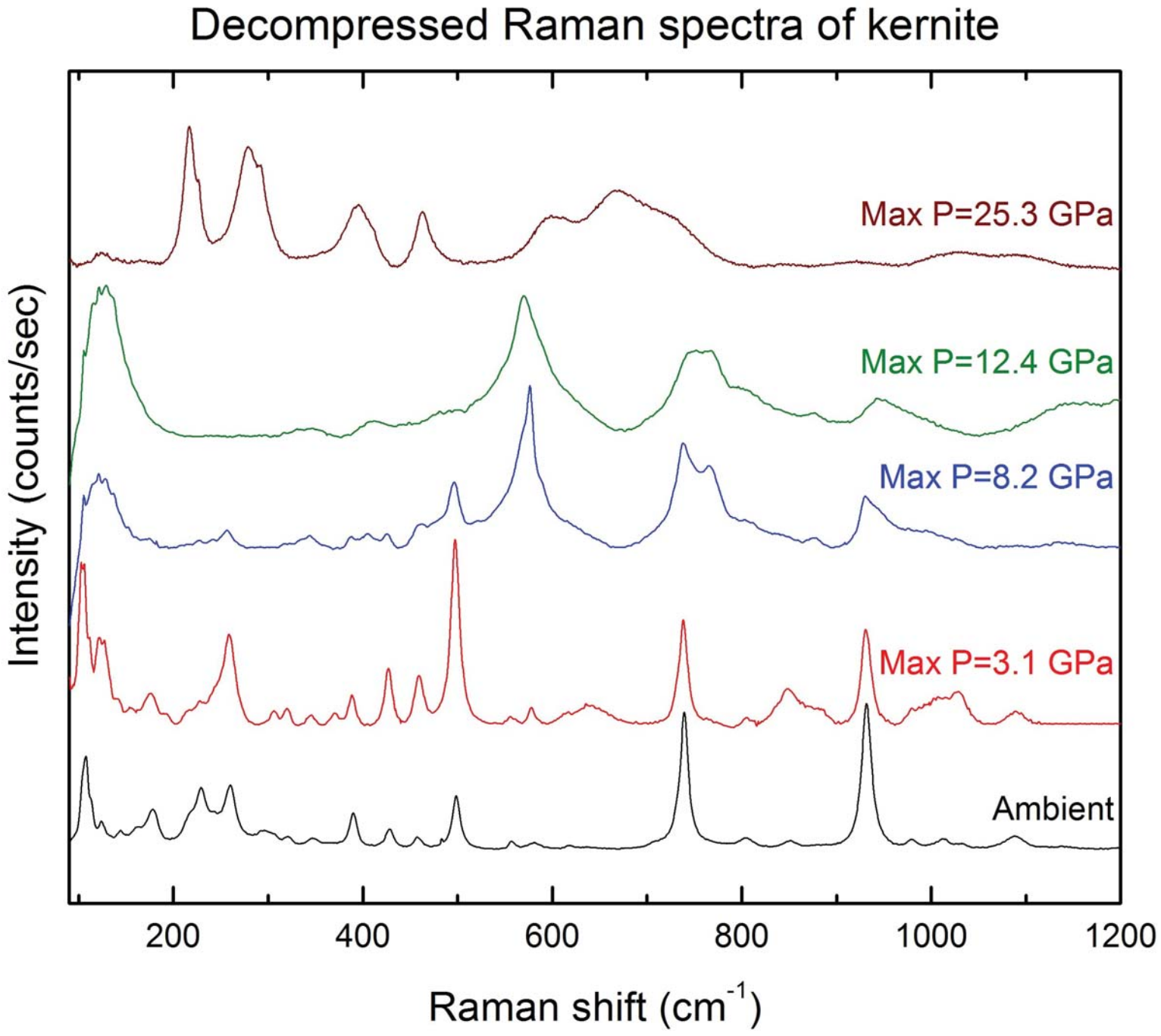

Always consult and cite the final, published document. See http:/www.minsocam.org or GeoscienceWorld

This is a preprint, the final version is subject to change, of the American Mineralogist (MSA)
Cite as Authors (Year) Title. American Mineralogist, in press.
DOI: https://doi.org/10.2138/am-2018-6253

Figure 12

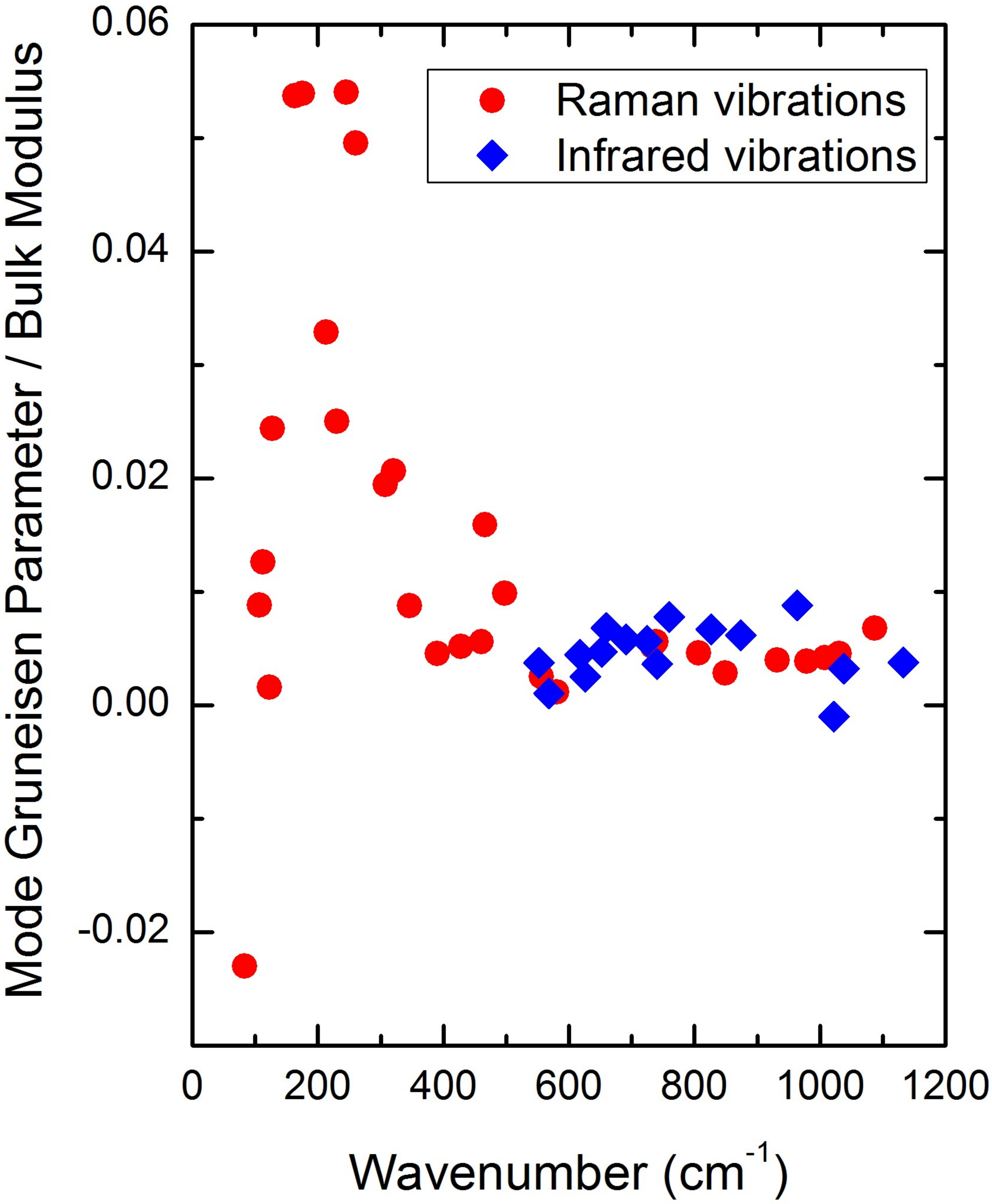

Always consult and cite the final, published document. See http:/www.minsocam.org or GeoscienceWorld

This is a preprint, the final version is subject to change, of the American Mineralogist (MSA)
Cite as Authors (Year) Title. American Mineralogist, in press.
DOI: https://doi.org/10.2138/am-2018-6253

ν_{0i} (cm^{-1})	Assignment	($d\nu_{0i}/dP$) to 2.5GPa (cm^{-1}/GPa)
83*	Na-O	-1.91 (±0.27)
107	Na-O	0.94 (±0.47)
113	Na-O	1.42 (±0.14)
123	Na-O	0.20 (±0.39)
128	Na-O	3.13 (±1.26)
163		8.78 (±0.88)
175		9.46 (±0.31)
214		7.02 (±1.38)
230		5.76 (±0.75)
246		13.28 (±1.28)
260		12.90 (±1.04)
308		5.98 (±1.80)
321		6.63 (±0.20)
346		3.05 (±0.12)
390	δ BO_4	1.79 (±0.18)
428	BO_4	2.23 (±0.43)
461	BO_4	2.58 (±0.11)
466	δ BO_3	7.43 (±1.24)
498	δ BO_3	4.92 (±0.54)
557	O-H Libration	1.41 (±0.31)
581	O-H Libration	0.69 (±0.43)
733	ν_s BO_4	3.82 (±0.49)
739	ν_s BO_4	4.16 (±0.37)
807	ν_s BO_4	3.73 (±0.72)
850	ν_s BO_4	2.42 (±0.39)
932	ν_s BO_3	3.73 (±0.64)
979		3.80 (±0.73)
1008		4.23 (±0.54)
1031	ν_{as} BO_4	4.69 (±0.71)
1088		7.41 (±0.81)
3004	H_2O	-
3255	H_2O	-
3301	H_2O	-
3351	H_2O	-
3425	H_2O	-
3548	OH stretch	-9.20 (±1.05)

Always consult and cite the final, published document. See http:/www.minsocam.org or GeoscienceWorld

This is a preprint, the final version is subject to change, of the American Mineralogist (MSA)
Cite as Authors (Year) Title. American Mineralogist, in press.
DOI: https://doi.org/10.2138/am-2018-6253

ν_{0i} (cm^{-1})	Assignment	($d\nu_{0i}/dP$) to 2.5 GPa (cm^{-1}/GPa)
552.3	BO_4	2.07 (±0.17)
568.4	BO_4	0.60 (±0.38)
618.0	δ BO_3	2.77 (±0.76)
626.3*		1.58 (±0.17)
652.7	δ BO_3	3.09 (±0.19)
659.7*		4.50 (±0.95)
691.2	δ BO_3	4.04 (±0.11)
724.5		4.14 (±0.38)
740.8		2.70 (±0.37)
760.1	ν_s BO_4	5.94 (±2.05)
826.7	ν_s BO_4	5.56 (±0.26)
874.1	ν_s BO_3	5.42 (±0.59)
963.6	ν_{as} BO_4	8.51 (±0.47)
1022.1	ν_{as} BO_4	-1.02 (±2.90)
1038.2*		3.38 (±0.75)
1132.7		4.28 (±0.62)
1260.5*		1.33 (±0.88)
1284.4		4.25 (±0.81)
1341.6	ν_{as} BO_3	5.15 (±0.44)
1387.8		-2.24 (±0.50)
1434.0		1.05 (±1.86)
1486.9		1.80 (±0.33)
1701.9	δ H-O-H	-17.58 (±0.67)
3323.2	H_2O	-7.78 (±5.67)
3551.4	OH	-13.63 (±2.20)

Always consult and cite the final, published document. See http:/www.minsocam.org or GeoscienceWorld

This is a preprint, the final version is subject to change, of the American Mineralogist (MSA)
Cite as Authors (Year) Title. American Mineralogist, in press.
DOI: https://doi.org/10.2138/am-2018-6253

ν_{0i} (cm^{-1})	Assignment	Raman (R) Infrared (IR)
124.0	Na-O	R
168.2	Na-O	R
217.3		R
226.1 sh		R
279.3		R
290.8 sh		R
395.3		R
410.3 sh		R
462.5	δ BO_3 & BO_4	R
598.3	δ BO_3 & BO_4	R
667.1		R
672.0		IR
735.5	ν_s BO_4	R
833.5	ν_s BO_4	IR
971.0	ν_{as} BO_4	IR
1073.9	ν_{as} BO_4?	IR
1127.8 sh	ν_{as} BO_4	IR
1198.9		IR
1272.4		IR
1368.0	ν_{as} BO_3	IR
1477.6		IR

Always consult and cite the final, published document. See http:/www.minsocam.org or GeoscienceWorld